Journal of Hydrology

A Bimodal Extension of the ARYA&PARIS Approach for Predicting Hydraulic Properties of Structured Soils

--Manuscript Draft--

Manuscript Number:	
Article Type:	Research paper
Keywords:	Pedotransfer functions, bimodal hydraulic properties, soil structure, hydraulic properties variability, soil water retention, soil hydraulic conductivity
Corresponding Author:	Shawkat Basel Mostafa Hassan, MSc University of Basilicata: Universita degli Studi della Basilicata Potenza, Potenza ITALY
First Author:	Shawkat Basel Mostafa Hassan, MSc
Order of Authors:	Shawkat Basel Mostafa Hassan, MSc
	Giovanna Dragonetti
	Alessandro Comegna
	Asma Sengouga
	Nicola Lamaddalena
	Antonio Coppola
Abstract:	The main purpose of this paper is to develop a bimodal pedotransfer function to obtain soil water retention (WRC) and hydraulic conductivity (HCC) curves. The proposed pedo-transfer function (PTF) extends the Arya and Paris (AP) approach, which is based on particle size distribution (PSD), by incorporating aggregate-size distribution (ASD) into the PTF to obtain the bimodal WRC. A bimodal porosity approach was developed to quantify the fraction of each of the porous systems (matrix and macropores) in overall soil porosity. Saturated hydraulic conductivity, K_0, was obtained from WRC using the Kozeny-Carman equation, whose parameters were inferred from the behaviour of the bimodal WRC close to saturation. Finally, the Mualem model was applied to obtain the HCC. In order to calibrate the PTF, measured soil physical and hydraulic properties data were used, coming from field infiltration experiments from an irrigation sector of 140 ha area in the “Sinistra Ofanto” irrigation system in Apulia, southern Italy. The infiltration data were fitted by using both bimodal and unimodal hydraulic properties by an inverse solution of the Richards equation. The bimodal “measured” hydraulic properties were then used to calibrate the scaling parameter (α_{AP}) of the proposed bimodal AP ($_{bim}AP$) PTF. Similarly, for the sake of comparison with the bimodal results, the unimodal hydraulic properties were used to calibrate the α_{AP} of the classical unimodal AP ($_{unim}AP$) PTF. Compared to the $_{unim}AP$ PTF, the proposed $_{bim}AP$ significantly improves the predictions of the mean WRC parameters and K_0, as well as the prediction of the shape of the whole HCC. Moreover, compared to the unimodal approach, it also allows keeping the hydraulic parameters’ spatial variability observed in the calibration dataset. Multiple linear regression (MLR) was also applied to analyse the sensitivity of the bimodal α_{AP} parameter to textural and structural features, confirming significant predictive effects of soil structure.
Suggested Reviewers:	Yakov Pachepsky yakov.pachepsky@usda.gov
	Horst Gerke gerke@zalf.de
	Angelo Basile angelo.basile@cnr.it
	Mario Palladino mario.palladino@unina.it
	Keith Smettem

	Keith.Smettem2@murdoch.edu.au

A BIMODAL EXTENSION OF THE *ARYA&PARIS* APPROACH FOR PREDICTING HYDRAULIC PROPERTIES OF STRUCTURED SOILS

Shawkat B.M. Hassan[a*], Giovanna Dragonetti[b], Alessandro Comegna[a], Asma Sengouga[a], Nicola Lamaddalena[b], Antonio Coppola[a]

[a] School of Agricultural, Forestry, Food and Environmental Sciences (SAFE), University of Basilicata, Viale dell'Ateneo Lucano, 10, 85100 Potenza PZ, Italy

[b] Mediterranean Agronomic Institute, Land and Water Division, IAMB, 70010 Valenzano BA, Italy

* Correspondence: Shawkat.hassan@unibas.it; Tel.: +39 348 253 1082

Abstract: The main purpose of this paper is to develop a bimodal pedotransfer function to obtain soil water retention (WRC) and hydraulic conductivity (HCC) curves. The proposed pedo-transfer function (PTF) extends the Arya and Paris (AP) approach, which is based on particle size distribution (PSD), by incorporating aggregate-size distribution (ASD) into the PTF to obtain the bimodal WRC. A bimodal porosity approach was developed to quantify the fraction of each of the porous systems (matrix and macropores) in overall soil porosity. Saturated hydraulic conductivity, K_0, was obtained from WRC using the Kozeny-Carman equation, whose parameters were inferred from the behaviour of the bimodal WRC close to saturation. Finally, the Mualem model was applied to obtain the HCC. In order to calibrate the PTF, measured soil physical and hydraulic properties data were used, coming from field infiltration experiments from an irrigation sector of 140 ha area in the "Sinistra Ofanto" irrigation system in Apulia, southern Italy. The infiltration data were fitted by using both bimodal and unimodal hydraulic properties by an inverse solution of the Richards equation. The bimodal "measured" hydraulic properties were then used to calibrate the scaling parameter (α_{AP}) of the proposed bimodal AP (*bimAP*) PTF. Similarly, for the sake of comparison with the bimodal results, the unimodal hydraulic properties were used to calibrate the α_{AP} of the classical unimodal AP (*unimAP*) PTF. Compared to the *unimAP* PTF, the proposed *bimAP*

Abbreviations: AP, Arya and Paris model; *bimAP*, bimodal Arya and Paris model; *unimAP*, unimodal Arya and Paris model

* Corresponding author.
E-mail address: Shawkat.hassan@unibas.it

significantly improves the predictions of the mean WRC parameters and K_0, as well as the prediction of the shape of the whole HCC. Moreover, compared to the unimodal approach, it also allows keeping the hydraulic parameters' spatial variability observed in the calibration dataset. Multiple linear regression (MLR) was also applied to analyse the sensitivity of the bimodal α_{AP} parameter to textural and structural features, confirming significant predictive effects of soil structure.

Keywords: Pedotransfer functions, bimodal hydraulic properties, soil structure, hydraulic properties variability, soil water retention, soil hydraulic conductivity

1. Introduction

The basis for understanding and solving agro-environmental problems increasingly lies in the use of agro-hydrological models. Such models frequently rely on mechanistic descriptions of fundamental processes involved in water and solute transport in soils (Abrahamsen and Hansen, 2000; Coppola et al., 2019; Šimůnek et al., 2008; Van Dam et al., 1997). Richards' equation (RE) and the Advection-Dispersion equation (ADE) are generally used for water flow and solute transport, respectively. Solving RE requires that soil water-pressure head, $\theta(h)$, and hydraulic conductivity-water content, $K(\theta)$, functions be specified at the space scale of concern. For large-scale applications, large hydraulic properties datasets are required to characterize the high spatial (and temporal) variability of soil hydraulic properties naturally found in extensive areas (Coppola et al., 2009a; Sposito, 1998). This is one of the more frustrating problems for soil scientists and hydrologists, because direct measurements are cumbersome and expensive, and may represent the main limit to using mechanistic models for large scale applications. This is also the chief justification for the use of simpler approaches (bucket approach, for example) than the RE.

In attempts to overcome this problem, in recent decades great efforts have been made to develop methods to estimate soil hydraulic properties from simpler data in the case of extensive direct characterizations. Since hydraulic properties are affected by other physical, chemical and biological properties, which are considered easier and cheaper to measure, empirical relations to predict them have been proposed. Most of these expressions can be classified as pedotransfer functions (PTFs, after Bouma, 1987) as they translate "readily" available information into the properties needed to solve RE. Continuous PTFs (Rawls and Brakensiek, 1985; Minasny et al., 1999) that calculate hydraulic properties from particle size distribution and additional soil variables such as bulk density via a mathematical relationship are being constantly improved. Neural network analysis has also been used to generate empirical PTFs (Schaap and Bouten, 1996). Leij et al. (2004) extended the use of neural networks by introducing terrain attributes. Overviews of the current status of PTF approaches are given by Basile et al. (2019) and Pachepsky et al. (2004).

Particle size distribution (PSD) data have also been used as a basis for estimating soil water retention using semi-physical PTFs (Haverkamp and Parlange, 1986). Arya and Paris (1981) significantly contributed to the expansion and spread of the approach. Their physico-empirical approach is mainly based on the similarity between shapes of the cumulative PSD and $\theta(h)$ curves. The model originally developed was refined (Arya et al., 1999a), also after later investigations (e.g., Basile and D'Urso, 1997), suggesting improvements pertaining to the limited flexibility of the formulation. Arya et al. (1999b) also derived an expression to compute $K(\theta)$ directly from PSD, based on the same soil structure model leading to the $\theta(h)$ relationship (Arya et al., 1999a; Arya and Paris, 1981). Hereafter, such an approach will be referred to as an AP approach.

Although the performance of PTFs for the retention curve has continuously improved, due also to increasing database size, they have still to be much improved on at least two interrelated issues: 1) ability to accurately predict saturated/unsaturated hydraulic conductivity; 2) ability to predict the spatial variability naturally found in measured soil hydraulic properties.

1) As for the issue of saturated hydraulic conductivity, K_0, Loague (1992) used textural-based K_0 estimates in a rainfall-runoff model to be applied in a small catchment and concluded that texture

was not a substitute for actual K_0 field data. Sobieraj et al. (2001) compared the performance of nine PTFs for estimating K_0 in modelling the storm flow generated in a rainforest catchment. They concluded that the PTFs used generally underestimated measured K_0, thus inadequately predicting hydrograph attributes, and grossly overestimating total runoff and peak runoff for almost all the events they examined. Tietje and Hennings (1996) tested six different PTFs and found different accuracy in the results between soils from the US and soils from Germany. Their study also showed that the prediction of K_0 using PTFs is inaccurate including the mean values of K_0 and their geometric standard deviation, especially for clay and silt soils. Vereecken et al. (2010) studied the use of PTFs to estimate van Genuchten and Mualem parameters. Their results showed inaccuracy in estimating hydraulic conductivity parameters using texture-based PTFs. A likely reason for this failure is that saturated hydraulic conductivity is largely dependent on soil structure and that currently used PTFs do not adequately (or at all) account for macroporosity in soils. The characteristics of macropores (mostly interaggregate pores) are not related to soil texture, such that soils with similar texture may have completely different saturated hydraulic conductivity (Coppola et al., 2009b; Pachepsky et al., 2004; Vereecken et al., 2010).

Besides on K_0, excluding the macropore information in a PTF may have an impact even on the shape of the whole HCC, especially when models based on the Hagen-Poiseuille, such as Mualem's conductivity model (Mualem, 1976), are used to predict hydraulic conductivity starting from the WRC. Actually, almost all of the existing PTFs assume pore systems with unimodal pore size distributions. This is justified by the fact that these PTFs have been calibrated by using datasets with either limited or no measurements at all close to saturation, which hold the information on the soil structure. The van Genuchten (1980) model is widely adopted to parametrize the unimodal WRC. Using the van Genuchten parameters in the Mualem model, estimation of the hydraulic conductivity is obtained by using the measured K_0 as matching factor. By contrast, when data close to saturation are available, a macropore portion of the water retention curve becomes frequently evident, which may require a bimodal model to be correctly described (Coppola, 2000; Coppola et al., 2009a, 2009b; Durner, 1994; Othmer et al., 1991; Ross and Smettem, 1993; Wilson et al., 1992). In all of the above papers, it has been shown that using either a unimodal or a bimodal model to describe WRC may induce significant changes in the prediction of the whole HCC. This is because, as discussed by Durner (1994) and shown experimentally by Coppola (2000), the formulation itself of Mualem's conductivity model makes the model particularly sensitive to the slope of the retention curve near saturation. This subject has received considerable theoretical and experimental treatment which shows that relatively small variations in water content close to saturation may be amplified by the algorithm for determining hydraulic conductivity (Coppola, 2000; Van Genuchten and Nielsen, 1985; Vogel and Cislerova, 1988).

2) As for the issue of spatial variability, which is strictly related to the issue described above, most of the studies around PTFs have focused more on the predictive capability of the mean values of hydraulic parameters than on their spatial variability. Much rarer are the attempts to evaluate the ability of PTFs to describe the spatial variability of soil hydraulic properties (Espino et al., 1996; Romano and Santini, 1997; Leij et al., 2004). Coppola et al. (2013) found that Rosetta PTF-based hydraulic parameters resulted in very low variability compared to the measured hydraulic parameters (see graphs 5 and 6 and tables 1 and 2 in their paper). This was especially true for the α and K_0 parameters of the van Genuchten-Mualem model (van Genuchten, 1980), which are known to be the parameters mainly related to the soil structure. The authors ascribed this behaviour to the fact that even in a quite homogeneous soil from a textural perspective, the structure may induce a variability in the soil hydraulic parameters which cannot be reproduced by PTFs not including explicitly structural information. Additionally, for the reasons already discussed above, the use of a unimodal model to describe bimodal porous media may also contribute to flatten the variability observed in the measurements.

Earlier efforts to properly account for macroporosity were mainly oriented to introducing additional information in PTFs explicitly considering macropore sizes and counts (McKeague et al., 1982; Nimmo et al., 2007). As also argued by Pachepsky and Rawls (2003), these studies showed that there is a potential usefulness in using aggregate size distribution in PTFs to improve water retention and hydraulic conductivity estimates.

Based on these premises, the aim of this study was to propose a bimodal extension of the AP approach (hereafter *bimAP*), which incorporates information on aggregate size distribution, to improve the prediction of the hydraulic properties and their spatial variability for structured soils. A large dataset of in situ infiltration measurements was used to establish the bimodal nature of hydraulic properties. Compared to the original AP model (hereafter *unimAP*), the *bimAP* model requires additional measurements of aggregate size distribution (ASD) and single-aggregate bulk density. Also, the *bimAP* water retention estimates require fitting by a bimodal water retention model to obtain the *bimAP* scaling parameter. A multiple linear regression was applied to analyse the degree of dependence of this scaling parameter on the textural and structural information. All the estimates from the *bimAP* were compared to those from the *unimAP*, to show the effects of not considering the effects of the structure on the predictions of the hydraulic properties and their spatial variability.

2. Materials and Methods

2.1. Hydraulic property models

In this paper, we use water retention models assuming pore systems with either unimodal or bimodal pore-size distributions. The van Genuchten (van Genuchten, 1980) model for unimodal porous systems is as follows:

$$S_e = \frac{\theta - \theta_r}{\theta_0 - \theta_r} = [1 + |\alpha_{VG} h|^n]^{-m} \qquad h<0$$
$$\theta = \theta_s \qquad h\geq 0 \tag{1}$$

where h is the pressure head ($h \leq 0$), S_e is effective saturation and θ is the water content (θ_s and θ_r are the water content at h=0 and for $h \to \infty$, respectively). α_{VG} (cm^{-1}), n and m=1-1/n are shape parameters. The effective saturation, S_e, may be considered a cumulative distribution function of pore size with a density function $f(h)$ which may be expressed by:

$$f(h) = \frac{dSe}{dh} \tag{2}$$

The presence of aggregates frequently results in a retention function curve with at least two inflection points. To represent such behaviour, a double porosity approach can be used which assumes that the pore space from θ_r to θ_s consists of two pore-size distributions, each occupying a fraction W_i of that pore space (Coppola, 2000; Durner, 1994). The model proposed by Durner (1994) is as follows:

$$S_e = \sum \beta_i \left[\frac{1}{1+(\alpha_{VG,i} h)^{n_i}}\right]^{m_i} \quad 0 < \beta_i < 1 \text{ and } \sum \beta_i = 1 \quad i = 1,2 \tag{3}$$

in which β_1 and β_2 are the weighting of the total pore space fraction to be attributed respectively to inter-aggregate pores (the macropores) and intra-aggregate pores (the micropores or matrix pores), and $\alpha_{VG,i}$, n_i and m_i still represent the fitting parameters for each of the partial curves.
The unsaturated hydraulic conductivity function is described by using the Mualem model (Mualem, 1976). It is based on the capillary bundle theory and relates relative hydraulic conductivity, K_r, to the pore-size distribution function $f(h)$ with the equation:

$$K_r(h) = \frac{K(h)}{K_0} = S_e^{\tau}[\eta(h)/\eta(0)]^2$$
$$\eta(h) = \int_{-\infty}^{\infty} h^{-1} f(h) dh \tag{4}$$

in which τ is a parameter accounting for the dependence of the tortuosity and the correlation factors on the water content. τ was fixed at a value of 0.5. The relative hydraulic conductivity is thus scaled using the saturated hydraulic conductivity, K_0 (hydraulic conductivity at h=0), as matching factor.

In the case of the unimodal van Genuchten model and assuming m=1-1/n, K_r becomes

$$K_r(S_e) = \frac{K(S_e)}{K_0} = S_e^{\tau}\left[1 - \left(1 - {S_e}^{1/m}\right)^{m}\right]^2 \tag{5}$$

In the case of bimodal Durner water retention, equation (5) becomes equation (6) (Priesack and Durner, 2006).

$$K_r(S_e) = \frac{K(S_e)}{K_0} = \left(\sum_{i=1}^{2} \beta_i S_{e,i}\right)^{\tau} \left\{\frac{\sum_{i=1}^{2} \beta_i \alpha_i \left[1 - \left(1 - S_{e,i}^{1/m_i}\right)^{m_i}\right]}{\sum_{i=1}^{2} \beta_i \alpha_i}\right\}^2 \tag{6}$$

2.2. Developing the Bimodal Arya and Paris approach for soil water retention

This section is devoted to describing in detail the *bimAP* approach. For the *unimAP* approach, the sequence of steps to obtain water retention curves by applying its classical concepts may be found in Arya and Paris (1981). We only recall here that it assumes cylindrical pores which are built by overlying the single particles (coming from the PSD) in a given size range.

In developing the *bimAP* approach, the main assumption is that the *unimAP* approach may be extended also to the ASD. Specifically, in the *bimAP* case, the total porous system is assumed to be partitioned into structural pore space (macropores, arising from particle aggregation) and matrix pore space (micropores, the only pores classically considered by the *unimAP*). Similar to matrix, which in the *unimAP* are ideally cylindrical and come from the overlying of the single particles of the PSD, the pores of the structural part of the porous system are also assumed to be cylindrical and simply built by overlying the aggregates in a given size range.

We will consider two cases: 1) the whole sample only consists of an ensemble of aggregates, without particle inclusions in the interspace among aggregates (see Figure 1a); 2) the whole sample consists of an ensemble of aggregates with particle inclusions in the interspace among aggregates (see Figure 1b).

Figure 1

In the *bimAP* approach, the porosity of the soil sample was divided into two porosities: macropore porosity (or structural porosity) which occupies the space between the aggregates, and matrix porosity which occupies the space between soil particles.

Below we give definitions and calculations, first for the single aggregate and then for the whole soil sample, which will be used in the *bimAP* approach applied to both the PSD and ASD.

i) Single aggregate

Let us start from the calculations for a single aggregate (one of the red clods in figure 1a and 1b). The aggregate will consist of solid particles and matrix pores (intra-aggregate pores). Below, the label *ag* is used for single aggregates.

The volume of solid particles in a single aggregate, assuming that the particle density ρ_s=2.65 g/cm^3, is:

$$v_{ag,prt} = \frac{w_{ag,prt}}{2.65} \tag{7}$$

where $w_{ag,prt}$ = dry weight of the aggregate = dry weight of the particles in the aggregate

The total volume of the aggregate is:

$$v_{ag,t} = v_{ag,prt} + v_{ag,p} \tag{8}$$

where $v_{ag,p}$ = volume of pores in the aggregate (determined by the ethyl alcohol method, see section *2.4*).

The bulk density of the aggregate, which will be used in the calculations for the whole sample, is:

$$\frac{w_{ag,prt}}{v_{ag,t}} = \rho_{b,ag} \tag{9}$$

Finally, the porosity of the aggregate is:

$$\frac{v_{ag,p}}{v_{ag,t}} = \varphi_{ag} \tag{10}$$

ii) Sample (ensemble of aggregates, without particle inclusions in the interspace among aggregates) (figure 1a)

In this case, it is assumed that all the sample weight consists of aggregates (no single particles leaving the finest sieve for aggregates). In the following, label *S* stands for sample.

The bulk density, $\rho_{b,S}$ and total porosity, $\Phi_{S,T}$, of the sample are:

$$\rho_{b,S} = \frac{W_{S,T}}{V_{S,T}}$$

(11)

$$\Phi_{S,T} = 1 - \frac{\rho_{b,S}}{2.65}$$

where $W_{S,T}$ is the total dry weight of particles in the sample and $V_{S,T}$ the total volume of the soil sample.

The volume occupied by the aggregates, $V_{S,AG}$, and by the inter-aggregate pores, in the soil sample (respectively the red and blue parts in figure 1) is:

$$V_{S,AG} = \frac{W_{S,T}}{\rho_{b,ag}}$$

(12)

$$V_{S,MCp} = V_{S,T-V_{S,AG}}$$

In equation (12), note that we use the bulk density of the aggregates determined on the single aggregate. We assume that $W_{S,T}$ is also the weight of the aggregates in the soil sample (no particle inclusion).

The inter-aggregate porosity, $\Phi_{S,MCp}$, and the intra-aggregate or matrix porosity, $\Phi_{S,MXp}$, are:

$$\Phi_{S,MCp} = \frac{\mathrm{V}_{S,MCp}}{V_{S,T}}$$

$$\Phi_{S,MXp} = \Phi_{S,T} - \Phi_{S,MCp} \tag{13}$$

$\phi_{\mathrm{S,MCp}}$ and $\phi_{\mathrm{S,MXp}}$ will be used, respectively, as saturated water contents for the structural part and for the matrix part of the water retention curve obtained by the AP method applied to both the aggregates and the particles (see section *iv.* below *bimAP approach for calculating the pore-spaces, capillary radius, pressure head and water contents for each class of particles or aggregates*).

The volume of the intra-aggregate pores (matrix pores), $\mathrm{V}_{S,MXp}$, and that of the solid particles, $\mathrm{V}_{S,prt}$, in the soil sample are:

$$\mathrm{V}_{S,MXp} = \Phi_{S,T} V_{S,T} - \mathrm{V}_{S,MCp}$$

$$\mathrm{V}_{S,prt} = V_{S,T} - \mathrm{V}_{S,MCp} - \mathrm{V}_{S,MXp} \tag{14}$$

The matrix particle density, $\rho_{S,prt}$, and the aggregate density, $\rho_{S,AG}$, are respectively:

$$\rho_{S,prt} = \frac{W_{S,T}}{V_{S,prt}}$$

$$\rho_{S,AG} = \rho_{b,ag} = \frac{W_{S,T}}{V_{S,AG}} = \frac{W_{S,T}}{V_{S,prt} + \mathrm{V}_{S,MXp}} \tag{15}$$

Note that in equation (15), $\rho_{S,AG}$ corresponds to the density $\rho_{b,ag}$ determined on the single aggregates.

Finally, from equations (14), one can define the void index of the whole sample, e_S, the void index coming from the pores in the aggregates (intra-aggregate pores = micro-pores), e_{SMX}, and the void index from the pores among the aggregates (inter-aggregate pores = macro-pores), e_{MC}:

$$e_S = \frac{V_{S,MCp} + V_{S,MXp}}{V_{S,prt}}$$

$$e_{MX} = \frac{V_{S,MXp}}{V_{S,prt}} \tag{16}$$

$$e_{MC} = \frac{V_{S,MCp}}{V_{S,prt}}$$

iii. Sample (ensemble of aggregates with particle inclusions in the interspace between aggregates) (figure 1b)

In this case, we assume that the inclusions (the orange particles) in the inter-aggregate space consist of single particles just occupying a part of this but without an inner porosity. The total weight of the sample does not correspond to the total weight of the aggregates. The latter corresponds to a fraction ε of the total weight. The inclusions occupy a space, $V_{S,MCprt}$, which is the volume of solid particles included in the inter-aggregate space.

In this case, the part of the total volume occupied by the aggregates in the soil sample (the red part in figure 1b) is:

$$V_{S,AG} = \frac{\varepsilon W_{S,T}}{\rho_{b,ag}} \tag{17}$$

Note that, as in equation (12), we use the bulk density of the aggregates determined on the single aggregate. We assume that $\varepsilon W_{S,T}$ is the weight of the aggregates in the soil sample.

Now, the total volume of inter-aggregate pores is:

$$V_{S,MCp} = V_{S,T} - V_{S,AG} - V_{S,MCprt} \tag{18}$$

where $V_{S,MCprt} = \frac{W_{S,T} - \varepsilon W_{S,T}}{2.65}$ = volume of the inclusions in inter-aggregate space. The remaining calculations for $\Phi_{S,MCp}$ and $\Phi_{S,MXp}$ are as for the no-inclusions case.

iv. bimAP approach for calculating pore spaces, capillary radius, pressure head and water contents for each class of particles or aggregates

As for the matrix pores, also the pores of the structural part of the porous system are assumed to be cylindrical and simply built by overlying the aggregates in a given size range.

All the calculations require that PSD and ASD (both expressed as percentages) be divided into a number of *N* radius classes.

Should only a negligible fraction of the air-dried soil sample be left in the smaller sieve for the aggregates, the case *ii. Sample (ensemble of aggregates, without particle inclusions in the interspace among aggregates)* will apply (this is our case in this paper). Of course, if this fraction were to be more significant, the approach would be simply extended by including its weight (1-ε) in the calculations (see case *iii. Sample (ensemble of aggregates with particle inclusions in the interspace among aggregates*).

In case *ii.*, the dry weight of the total number of single particles in the sample coincides with that of the total number of aggregates:

$$W_{S,T} = \sum_{i=1}^{N_{PSD}} W_{S,T,i_{R<1}} = \sum_{i=1}^{N_{ASD}} W_{S,T,i_{R>1}} \qquad (19)$$

where $W_{S,T,i_{R<1}}$ is the dry weight of the particles in the ith class of particles of radius R<1mm, $W_{S,T,i_{R>1}}$ is the dry weight of the aggregates in the ith class of aggregates of radius R>1mm, and N_{PSD} and N_{ASD} are the number of classes into which the PSD and ASD distribution are divided.

The volume of pores from the ith class of particles of radius R<1mm may be obtained as

$$V_{S,P,i_{R<1}} = \frac{W_{S,T,i_{R<1}} e_{MX}}{\rho_{S,prt}} = \frac{W_{S,T,i_{R<1}} e_{MX} \mathrm{V}_{S,prt}}{W_{S,T}} \quad (20)$$

where $\frac{W_{S,T,i_{R<1}}}{W_{S,T}}$ is the solid mass per unit sample mass in the i^th particle-size range. It is obtained by taking the differences in cumulative percentages corresponding to successive particle sizes divided by 100, such that the sum of $\frac{W_{S,T,i_{R<1}}}{W_{S,T}}$ for all the *n* classes is unity.

Similarly, the volume of pores from the i^th class of aggregates of radius R>1mm is:

$$V_{S,P,i_{R>1}} = \frac{W_{S,T,i_{R>1}} e_{AG}}{\rho_{S,AG}} = \frac{W_{S,T,i_{R>1}} e_{AG} \mathrm{V}_{S,AG}}{W_{S,T}} \quad (21)$$

where $\frac{W_{S,T,i_{R>1}}}{W_{S,T}}$ is the solid mass per unit sample mass in the ith aggregate-size range. Again, it is obtained by taking the differences in cumulative percentages corresponding to successive aggregate sizes divided by 100, such that the sum of the $\frac{W_{S,T,i_{R>1}}}{W_{S,T}}$ for all the *n* classes is unity.

By using equations (20) and (21), it is possible to calculate the water content in the matrix pores, $\theta_{S,i_{R<1}}$, and that in the macropores, $\theta_{S,i_{R>1}}$, as follows:

$$\theta_{S,i_{R<1}} = \frac{\sum_{j=1}^{i} V_{S,P,i_{R<1}}}{V_{S,T}}$$

$$(22)$$

$$\theta_{S,i_{R>1}} = \frac{\sum_{j=1}^{i} V_{S,P,i_{R>1}}}{V_{S,T}}$$

which are obtained respectively by progressively filling matrix (and macropore) volumes with water up to the selected i^th $V_{S,P,i_{R<1}}$volume (i^th $V_{S,P,i_{R>1}}$volume).

Now, the number of particles in the ith class of particles of radius R_i<1mm (all the particles in the range are assumed to form a single cylindrical pore of volume $V_{S,P,i_{R<1}}$) may be obtained as follows:

$$n_{i,prt} = \frac{3V_{S,P,i_{R<1}}}{4\pi R_i^3} \tag{23}$$

Similarly, the number of aggregates in the ith class of aggregates of radius R_i>1mm (all the aggregates in the range are assumed to form a single cylindrical pore of volume $V_{S,P,i_{R>1}}$) are calculated as:

$$n_{i,AG} = \frac{3V_{S,P,i_{R>1}}}{4\pi R_i^3} \tag{24}$$

The radius of the pores in the ith class of particles of radius R_i<1mm, $r_{i,MX}$, and the radius of the pores in the ith class of aggregates of radius R_i>1mm, $r_{i,AG}$, are:

$$\begin{aligned} r_{i,MX} &= R_i \frac{\left[4e_{MX} n_{i,prt}^{(1-\alpha_{MX})}\right]^{0.5}}{6} \\ r_{i,AG} &= R_i \frac{\left[4e_{MC} n_{i,AG}^{(1-\alpha_{MC})}\right]^{0.5}}{6} \end{aligned} \tag{25}$$

from which the pressure head for the radius of the pores in the ith class of particles of radius R_i<1mm, $h_{i,MX}$, and that corresponding to the radius of the pores in the ith class of aggregates of radius R_i>1mm, $h_{i,MC}$, may be calculated as follows:

$$h_{i,MX} = \frac{2\sigma cos\vartheta}{\rho_w g r_{i,MX}} \tag{26}$$

$$h_{i,MC} = \frac{2\sigma cos\vartheta}{\rho_w g r_{i,MC}}$$

where σ is water-air surface tension, ϑ is contact angle, ρ_w is density of water, and *g* is gravity acceleration.

α_{MX} and α_{MC} are scaling parameters for pore length, accounting for the fact that the actual soil particles and aggregates are not spherical. In their classical *unimAP*, Arya and Paris (1981) assumed the parameter α_{MX} to be >1 under the hypothesis that each particle contributes a length greater than the diameter of an equivalent sphere. As a first approximation, in our *bimAP* approach, we will assume that this hypothesis extends to α_{MC} and that the two parameters have the same value, such that $\alpha_{MX} = \alpha_{MC} = \alpha_{AP}$. Parameter α_{AP} has to be estimated by fitting the AP estimates to measured water retention curves for both the *unimAP* and *bimAP* cases (see section *2.7* below*. Fitting the AP estimates to the measured hydraulic properties to calibrate the* α_{AP} *parameter*).

The matrix and the macropore parts of the water retention are simply obtained by combining pairs of $\theta_{S,i_{R<1}}$- $h_{i,MX}$ and $\theta_{S,i_{R>1}}$- $h_{i,MC}$. Total water retention is obtained by summing up the two partial contributions (see the symbols in Figure 2).

Figure 2

v. Using the information from bimAP to estimate K_0

Saturated hydraulic conductivity, K_0, was obtained by using the following Kozeny-Carman equation (Kozeny, 1927; Carman, 1937):

$$K_0 = \eta \phi_e^{\gamma} \tag{27}$$

where ϕ_e is the effective porosity, which is the difference between the saturated water content and the water content at field capacity (330 cm matric suction), and η and γ are constants. All these parameters were estimated from the curve obtained by fitting the water retention model (whether unimodal or bimodal) to the AP estimates. Obviously, all the parameters in the Kozeny-Carman equation will change depending on the approach used (*unimAP* or *bimAP*).

In order to estimate the other parameters in equation (27), in our approach we used the version of the Kozeny-Carman equation proposed by Timlin et al. (1999):

$$\begin{gathered} K_0 = 0.0131\left(\frac{F}{l}\right)^{0.5} \varphi_e^{2.5} \\ F = 0.148/h_b \\ l = 1.86(2-\lambda)^{5.34} \end{gathered} \tag{28}$$

where F and l are parameters related to the fractal dimensions of porosity (Rawls et al., 1993), λ is the pore size distribution index, and h_b is the air-entry potential in the Brooks and Corey water retention model (BC model) (Brooks and Corey, 1964):

$$S_e = (\theta - \theta_r)/(\theta_s - \theta_r) = \left(\frac{h}{h_b}\right)^{\lambda} \tag{29}$$

In the case of bimAP, since K_0 is related to the water retention characteristics near saturation, λ and h_b were obtained by fitting the BC model to the upper part of the *bimAP* WRC. In the case of the *unimAP* approach, λ and h_b were estimated by fitting the BC model to the whole water retention curve.

2.3. The study area

The study area is sector 6 of irrigation district 10 in the "Sinistra Ofanto" irrigation system, which is located on the left bank of the Ofanto river in Puglia, Southeast Italy (see figure 3). The study sector covers an area of 140 hectares of agricultural land and is irrigated with an on-demand pressurized network. The whole district covers 22,500 hectares of agricultural land.

Figure 3

2.4. Measurement of soil physical parameters

The approach proposed in this paper assumes the bimodality of soil porosity. It requires measurement of the size distribution of the single particles (PSD), as well as the size distribution of the aggregates (ASD) present in an undisturbed soil sample.

Undisturbed soil samples were collected using steel cylinders 7 cm in diameter and 7 cm high in 90 sites selected in the study area (about 140 hectares). Additionally, some disturbed soil was also sampled to determine the average bulk density of single aggregates.

After measuring the sample volume, the undisturbed soil was removed from the sampler and air-dried for at least one week. Sieve analysis was carried out on each sample to obtain the ASD curve according to the dry-sieving method proposed by Nimmo & Perkins (2002). The sieve sizes used in this analysis were: 40, 31.5, 25, 20, 16, 10, 8, 5, 2 and 1 mm. All the soil remaining in a sieve was considered to consist of aggregates of a radius exceeding the sieve size. All the soil passing the narrowest sieve was kept. All the soil initially contained in a sampler was then oven-dried at 105 °C for 24 hours to determine bulk density, ρ_b, and thus PSD. Total porosity was calculated from the measured bulk density assuming that particle density was 2.65 g/cm^3. PSD curves were obtained by using the hydrometer method combined with sieve analysis to characterize the range of particle diameter from 2 up to 2000 μm (Gee and Or, 2002). The dry soil was lightly crushed on a tray using a rolling pin to break up clods until the soil passed through a 2 mm sieve. Fifty grams of the sieved soil were pre-treated with 30% (w/v) hydrogen peroxide until no reaction was revealed to remove organic matter. After washing and air-drying of residual soil, chemical dispersion of soil particles was achieved by mixing the soil sample with a 5 g L-1 sodium-hexametaphosphate (HMP) solution adjusted to pH 8.5, allowing the soil to soak overnight. Physical dispersion was obtained with mechanical mixing with an electric stirrer working at 10000 rpm. Then soil samples were transferred to 1000-mL sedimentation cylinders. After thorough mixing of soil suspension, the suspension density was measured and recorded after 3, 10, 30, 60, 210, 1440 minutes with an ASTM 152H. The hydrometer readings were also made at the same times on a blank solution to correct for the density of HMP solution. At the end of readings, the contents of the cylinder were poured out through a 45-μm sieve to retain coarser particles. The retained material was oven-dried for 24 h at 105 °C and sieved with a nest of sieves of 1000, 500, 250, 106, 53 μm. The portion of sand retained on each sieve was weighed and annotated. Following the above procedure, we determined a particle size distribution curve composed by 11 experimental points for all of the soil samples. Sand, silt and clay contents were expressed as percentages by mass of the fine-earth fraction (<2 mm). According to the USDA soil classification, the texture of the soil samples in the examined dataset ranged from silty-clay-loam to sandy-loam (see figure 4). Overall, the above methods allowed 20 points to be obtained for PSDs and 10 for ASDs.

Figure 4

Both PSD and ASD curves were described by a parametric (van Genuchten-type) equation:

$$P = 100 + (T_s - 100)(1 + (T_\alpha D)^{T_n})^{-T_m} \tag{30}$$

where P is the percentage of the particle or aggregate passing from a sieve size; D is the sieve size;

T_s, T_α, T_n and T_m are parameters similar to those of van Genuchten (1980) model, and T_m=1-1/T_n. The parameters were obtained by fitting equation (1) to the measured PSDs and ASDs (Figure 5).

Figure 5

The average bulk density of the single aggregates was determined using the disturbed soil samples. As with undisturbed soil samples, the soil was left to air-dry for a week. Aggregates of different sizes were then selected, whose porosity was determined by using the ethyl alcohol method proposed by Moret-Fernandez and Lopez (2019). First, the dry aggregate was weighed. Then it was immersed in ethanol in a beaker, which was covered well with biofilm to avoid ethanol evaporation. The bubbling was observed for at least 20 minutes until it stopped, indicating aggregate saturation with ethanol. After saturation, the aggregate was carefully taken from ethanol and placed on a paper filter for less than 10 seconds before measuring its new weight. At the same time, the temperature of the alcohol was measured using a mercury thermometer in order to determine the alcohol density. This process was done for several aggregates from different locations and with different sizes at room temperature set to be less than 25 °C. Thus, the volume of the pores, V_p, was calculated as:

$$V_p = \frac{W_{agg-al} - W_{agg}}{\rho_{al}} \tag{31}$$

where W_{agg-al} is the weight of the aggregate after saturation with alcohol, W_{agg} is the dry weight of the aggregate, and ρ_{al} is the alcohol density. The volume of the solid phase, V_s, in the aggregate was then calculated as:

$$V_s = \frac{W_{agg}}{\rho_s} \tag{32}$$

where ρ_s is the solid particle density, which can be assumed to be 2.65 g/cm^3. Finally, the aggregate bulk density was calculated as follows:

$$\rho_{b,ag} = W_{agg}/(V_s + V_p) \tag{33}$$

2.5. Direct measurement of soil hydraulic parameters

Soil hydraulic parameters at each of the 90 studied sites were obtained using tension infiltrometers (Ankeny et al., 1988; Coppola et al., 2011). First, the soil surface was levelled. Then a ring was placed on the surface and a thin layer of homogeneous fossil sand was added to the soil surface to ensure good contact with the infiltrometer disc. At each site, infiltration experiments were carried out at four sequential water pressure head values (-15, -10, -5 and -1 cm). Water pressure was controlled by raising or lowering the tube in the bubble tower. A soil sample was taken before and after the infiltration process to measure the initial and final water content.

The cumulative infiltration data were used as input in an inverse solution of the 3D Richards equation to obtain both the unimodal and bimodal hydraulic property parameters by a parameter estimation procedure. The van Genuchten-Mualem and Durner-Mualem models were used to describe unimodal and bimodal hydraulic properties, respectively. As for the unimodal properties, they were estimated by using DISC software (Šimůnek and van Genuchten, 1996). Inverse solution using bimodal properties was carried out by using the software HYDRUS 2D/3D (Rassam *et al.*, 2003; Šimůnek *et al.*, 2008). In both cases, the saturated water content for each site was fixed at the total porosity, residual water content was fixed as zero, τ was fixed as 0.5, in order to minimize the number of variables to be optimized. Parameter m was assumed to be m=1-1/n for both the unimodal and the bimodal descriptions. The weight β_1 in the Durner model was assumed to be equal to the fraction of macroporosity to total porosity $\Phi_{S,MCp}/\Phi_{S,T}$. Eventually, the inverse solution would estimate the three parameters involved for the unimodal scenario (namely, α, n, *and* K_0) and five parameters for the bimodal scenario (namely: α_1, n_1, α_1, n_1, and K_0).

2.6. Akaike Information Criterion (AIC) to test the bimodality of the porous medium

The goodness of fit from the inverse solution for both the unimodal and bimodal scenarios was compared in order to test the bimodality of soil pores. The root-mean-square error (*RMSE*) was used as a measure of the distance between the predicted and the measured infiltrated depths (equation 35). Unimodal and bimodal scenarios involve a different number of parameters. The Akaike Information Criterion (AIC) was used to balance the goodness of fit and the number of parameters involved:

$$AIC = N_o \ln\left(\frac{RMSE}{N_o}\right) + 2k \tag{34}$$

$$RMSE = \sqrt{\frac{\sum_{i=1}^{N_o}(x_i - \hat{x})^2}{N_o}} \tag{35}$$

where N_o is the number of observations, k = the number of parameters + 1, x_i is the variable obtained from field measurements and $\hat{x}_i$ is the variable estimated from *unimAP* or *bimAP*. The lower the AIC, the better the fit.

2.7. Fitting AP estimates to the measured hydraulic properties to calibrate parameter α_{AP}

The proposed model is physically-based with one unknown parameter (both for *unimAP* and *bimAP*), which is the scaling parameter (α_{AP}). This parameter was estimated by fitting the *unimAP* and *bimAP* estimates to respectively the unimodal and bimodal measured water retention curves (see again the graph in figure 2).

2.8. Evaluating the dependence of parameter α_{AP} on textural and structural physical properties

Multiple linear regression (MLR) was applied to relate the scaling parameter α_{AP} to texture and aggregate properties with a view to predicting α_{AP} with only physical properties available and with no prior knowledge of the hydraulic parameters. The regression analysis included: 1) the parameters of the equations used to interpolate PSD and ASD (namely, T_s, T_n and T_α); 2) soil bulk density (ρ_b); 3) the fraction of the macropores from total porosity (β_1). The regression model was developed by using the hydraulic parameters obtained from the field measurements.

2.9. Schematic view of the approach used in the paper

For easier interpretation of the results of the *bimAP* application, Figure 6 summarizes the steps followed in this paper to test the *bimAP* PTF and to compare it to the *unimAP* approach. On the one hand, inverse solution of tension infiltration experiments was used twice to obtain the unimodal van Genuchten (van Genuchten, 1980) and the bimodal Durner (Durner, 1994) hydraulic properties. Hereafter, they will be called the measured hydraulic properties. The Akaike Information Criterion (AIC) was used to establish the bimodality of the hydraulic properties. On the other, both the unimodal and bimodal AP approaches were used to obtain, respectively, *unimAP* and *bimAP* estimates of the WRC. These were fitted respectively to the unimodal and bimodal measured WRC to obtain the scaling parameter (α_{AP}) for both the *unimAP* and *bimAP* approaches. Saturated hydraulic conductivity (K_0) was then estimated from both *unimAP* and *bimAP* WRCs using the Kozeny-Carman equation (Carman, 1937; Kozeny, 1927), and was subsequently used to obtain $K(h)$ curves (HCCs) using the Mualem model (Mualem, 1976; Priesack and Durner, 2006). Finally, multiple linear regression (MLR) was used to analyse the dependence of the scaling parameter, α_{AP}, on soil physical parameters.

Figure 6

3. Results and Discussion

3.1. Testing the bimodality of the measured hydraulic property dataset

Some results of the inverse solutions for three locations in the study area are shown in figure 7. The symbols represent the observed infiltration depths, while the solid lines represent the infiltration depths obtained from the inverse solution. Each plot on the left represents a unimodal inverse solution, whereas the corresponding right-hand plot represents the bimodal inverse solution for the same location. Figure 8 shows the results of AIC values for unimodal and bimodal inverse solutions for all 90 sites investigated.

Figure 7

Figure 8

Looking at both the graphs in figure 7 and the AIC values in figure 8, fitting infiltrated depths by using the bimodal model frequently gives better results than the unimodal model. AIC analysis shows that the bimodal model provides better estimates in almost 73% of the locations in the study area. These results allowed us to conclude that the hydraulic property dataset is mostly bimodal and is thus appropriate for calibrating the proposed *bimAP* PTF.

The first two columns in Table 1 show the average and the standard deviation of the parameters of the unimodal and bimodal hydraulic properties obtained from the measurements (subscript *meas*). It is worth noting that in the unimodal case the parameter K_0 is on average higher than the bimodal K_0, with also a much higher standard deviation. Moreover, the relatively high unimodal water retention parameter α would also indicate a quite low (in absolute value) air-entry pressure head, which is typical of sandy soils (which is not the case of the investigated soils). This behaviour may be ascribed to a fast infiltration rate observed during the infiltration experiments, which the unimodal model tries to capture by using relatively high values of α and K_0. The variability of the infiltration rate thus induces a high variability of the unimodal K_0. By contrast, the bimodal model explicitly includes additional parameters (α_1 and n_1), which allow rapid infiltration to be described as a swift emptying of the structural pores without the need to increase the saturated hydraulic conductivity excessively. Actually, in the bimodal case the variability observed in the infiltration rate is now fulfilled by the relatively high standard deviation of α_1 and n_1, whereas the variability of the bimodal K_0 remains quite limited. This should open a discussion on the real meaning of the high coefficient of variations generally found in the saturated hydraulic conductivity, especially when arising from inversion procedures, which could come partly from the inadequate model used for describing hydraulic properties in the presence of soil structure.

3.2. Comparing measured hydraulic properties and *unimAP* and *bimAP* estimates

The graphs in Figure 9 compare the measured WRC (solid lines - coming from the inversion of infiltration experiments) to those obtained by both the *unimAP* and *bimAP* (dashed lines) for three of the sites investigated. Figure 10 compares the corresponding HCCs. In both figures, the graphs on the left side show the comparison of unimodal measured and estimated curves, whereas those on the right compare the bimodal measured and estimated curves. All comparisons were carried out in terms of root-mean square error (RMSE).

We recall that the AP estimates are obtained from the optimization of a single parameter, namely the α_{AP} scaling parameter. Graphical results show that introducing the aggregate information in the *bimAP* significantly improves the ability of the approach to estimate soil water retention (with average RMSE values of 0.43 and 0.11 for *unimAP* and *bimAP*, respectively). Even more importantly, the WRC parameters obtained under the *bimAP* (the Durner parameters) and K_0 from the Kozeny-Carman model significantly improve hydraulic conductivity (with average RMSE values of 0.315 and 0.28 cm/min for *unimAP* and *bimAP*, respectively) predicted by applying the Mualem model.

The substantial enhancement of the K_0 estimates is apparent in Figure 11, showing a comparison of saturated hydraulic conductivity as measured and obtained by *unimAP* (empty triangles) and *bimAP* (solid triangles), with much smaller RMSE and scattering around the 1:1 line for the *bimAP* case (RMSE = 0.747) compared to *unimAP* (RMSE = 12.580).

The third and fourth columns in Table 1 show the average and the standard deviation of the hydraulic property parameters obtained from the AP PTF estimates (subscript *PTF*). It is worth noting in the table that the *unimAP* is unable to obtain either the average value of the saturated hydraulic conductivity, or its variability. As discussed by Coppola et al. (2009a, 2009b), PTFs tend to flatten the variability generally found in measured hydraulic properties. This is mostly due to the information on the structure being overlooked, as well as using unimodal models to describe the hydraulic properties of structured soils, when developing PTFs. This is clearly demonstrated by the parameter values for the *bimAP* approach given in the table, showing that accounting explicitly for the structure in developing PTFs allows much better estimates of K_0 and, importantly, its variability. The same may be said for all the parameters describing both the textural and structural parts of the water retention curve (see the average and standard deviations for n_1, α_2 and n_2 in table 1).

Figure 9

Figure 10

Figure 11

3.3. Relationship between the scaling parameter, α_{AP}, and soil physical properties

Multiple linear regression was used to evaluate the degree of dependence of the scaling factor α_{AP}

on soil physical parameters. This is especially important in view of using the *bimAP* PTF in soils where no references to measured hydraulic properties are available. Table 2 summarizes the coefficients and the intercepts of soil physical parameters to predict α_{AP} using MLR. The physical parameters used in the regression are: 1) the parameters of the PSD and ASD curves (see section *2.4. Measurements of soil physical parameters*), 2) soil bulk density, and 3) macropore fraction in the sample's overall porosity (β_1).

The values in the table show a relatively strong correlation of the scaling parameter with bulk density and the slope of the PSD curve (both in *unimAP* and *bimAP*). However, when the structure is explicitly taken into account (the *bimAP* case), a clear correlation emerges between α_{AP} and the aggregate parameters, namely $T_{\alpha,ASD}$ and the fraction of aggregate porosity to total porosity, β_1, which cannot be detected when a unimodal approach without structure is considered.

Improvement in the correlation with soil structural properties of *bimAP* is also apparent when plotting the α_{AP} values obtained by the MLR against the original values of α_{AP} for both the *unimAP* (white symbols) and *bimAP* (black symbols) approaches (see Figure 12). The RMSE is 0.418 and 0.227 for *unimAP* and *bimAP*, respectively. That said, regardless of the better overall description of the curves, *bimAP* always appropriately captures the behaviour close to saturation, which is crucial for predicting hydraulic conductivity and hydraulic property variability.

Figure 12

Conclusions

The main purpose of this paper was to develop a bimodal physically-based PTF to estimate soil hydraulic parameters. The proposed PTF (*bimAP*) is based on the principles of the Arya and Paris (1981) PTF, incorporating aggregate-size distribution to obtain bimodal soil hydraulic parameters. The proposed approach provides bimodal WRCs and HCCs starting from soil physical parameters:

PSD, ASD, sample bulk density, and single-aggregate bulk density.

Overall, *bimAP* provides better estimates of soil hydraulic parameters and their variability compared to the *unimAP* PTF. K_0, the whole shape of the HCC, as well as their variability, are better predicted by accounting for soil structure and bimodal porosity in the development of the PTF. In general, the *bimAP* approach produces hydraulic parameter estimates remaining within a more physically plausible region than in the *unimAP* approach. It also enhances the ability of MLR to predict the scaling parameter, α_{AP}.

Our results confirm that, in the perspective of PTF calibration for estimating K_0 and, more generally, the hydraulic conductivity function, the relevant information on the bimodal character of the porous medium included in the soil water retention near saturation must be described in detail. Unfortunately, unimodal hydraulic functions are unable to describe the transition between pore systems frequently indicated by the retention data in aggregated soils. Consequently, if a unimodal water retention function is used to fit measured retention data with a bimodal behaviour and then to calibrate PTF parameters, a poor performance of the PTFs is expected when used to estimate hydraulic conductivities.

From our data set, it may be observed that by introducing bimodality excellent AP estimates can be obtained for aggregated soils. Owing to the flexibility arising from the structural-matrix partition specifically built into the modified AP retention model, the *bimAP* estimates keep the fundamental information on soil aggregation in the measured soil water retention within the range of soil water potential near saturation, thus providing accurate predictions of pore size distribution and hence of the hydraulic conductivity curve.

Of course, to be effectively and reliably applied the bimodal approaches always require that the predominant effects of the soil hydrological behaviour near saturation be supported by accurate and detailed experimental descriptions of the retention curve and hydraulic conductivity for high water contents, which would allow less uncertain identification of the processes and related parameters involved.

Acknowledgements

This research was funded by MUR, protocol number 2017XWA834 (INtegrated Computer modeling and monitoring for Irrigation Planning in ITaly – INCIPIT).

References

Abrahamsen P., Hansen S., 2000. Daisy: an open soil-crop-atmosphere system model. Environ. Model. Softw. 15(3), 313–330. https://doi.org/10.1016/S1364-8152(00)00003-7

Arya, L.M., Leij, F.J., Shouse, P.J., Van Genuchten, M.T., 1999. Relationship between the hydraulic conductivity function and the particle-size distribution. [Erratum: Jan/Feb 2003, v. 67 (1), p. 373.]. Soil Sci. Soc. Am. J. 63, 1063–1070.

Arya L.M., Leij F.J., van Genuchten M.T., Shouse P.J., 1999. Scaling parameter to predict the soil water characteristic from particle-size distribution data. Soil Sci. Soc. Am. J., 63(3), 510–519. https://doi.org/10.2136/sssaj1999.03615995006300030013x

Arya L.M. and Paris J.F., 1981. A physicoempirical model to predict the soil moisture characteristic from particle-size distribution and bulk density data. Soil Sci. Soc. Am. J., 45(6), 1023–1030. https://doi.org/10.2136/sssaj1981.03615995004500060004x

Basile A., Bonfante A., Coppola A., De Mascellis R., Falanga Bolognesi S., Terribile F. and Manna P., 2019. How does ptf interpret soil heterogeneity? A stochastic approach applied to a case study on maize in northern Italy. Water, 11(2), 275–291. https://doi.org/10.3390/w11020275

Basile A., D'Urso G., 1997. Experimental corrections of simplified methods for predicting water retention curves in clay-loamy soils from particle-size determination. Soil Technol. 10(3), 261–272. https://doi.org/10.1016/S0933-3630(96)00020-7

Bouma J., 1987. Transfer functions and threshold values: from soil characteristics to land qualities. Workshop on Quantified Land Evaluation Process, Vol 6. : International Institute for Aerosphere Survey and Earth Science.

Brooks R., Corey T., 1964. Hydraulic properties of porous media. Hydrol. Pap. Colorado State univ. 3, 1 – 27

Carman P.,1937. Fluid flow through a granular bed. Trans. Inst. Chem. Eng. 15, 150–167

Coppola A., 2000. Unimodal and bimodal descriptions of hydraulic properties for aggregated soils. Soil Sci. Soc. Am. J. 64(4): 1252–1262. https://doi.org/10.2136/sssaj2000.6441252x

Coppola A., Basile A., Comegna A., Lamaddalena N., 2009. Monte Carlo analysis of field water flow comparing uni- and bimodal effective hydraulic parameters for structured soil. J. Contam. Hydrol. 104(1–4), 153–165. https://doi.org/10.1016/j.jconhyd.2008.09.007

Coppola A., Comegna V., Basile A., Lamaddalena N., Severino G., 2009. Darcian preferential water flow and solute transport through bimodal porous systems: Exp. Model. J. Contam. Hydrol. 104(1–4), 74–83. https://doi.org/10.1016/j.jconhyd.2008.10.004

Coppola A., Dragonetti G., Comegna A., Lamaddalena N., Caushi B., Haikal M.A., Basile A., 2013. Measuring and modeling water content in stony soils. Soil. Tillage. Res. 128, 9–22. https://doi.org/10.1016/j.still.2012.10.006

Coppola A., Dragonetti G., Sengouga A., Lamaddalena N., Comegna A., Basile A., Noviello N., Nardella L., 2019. Identifying optimal irrigation water needs at district scale by using a physically based agro-hydrological model. Water. 11, 841–865. https://doi.org/10.3390/w11040841

Durner W., 1994. Hydraulic conductivity estimation for soils with heterogeneous pore structure. Water. Resour. Res. 30(2), 211–223. https://doi.org/10.1029/93WR02676

Espino A., Mallants D., Vanclooster M., Feyen J., 1996. Cautionary notes on the use of pedotransfer functions for estimating soil hydraulic properties. Agric. Water. Manag,, 29(3), 235–253. https://doi.org/10.1016/0378-3774(95)01210-9

Gee G., Or D., 2002. Particle-size analysis. in: Dane J., Topp C. (Eds.), Methods of Soil Analysis, Part 4: Physical Methods. Soil Science Society of America Inc., Madison, WI, pp. 255–293

Haverkamp, R., Parlange, J.Y., 1986. Predicting the water-retention curve from particle-size distribution: 1. Sandy soils without organic matter. Soil. Sci., 142(6), 325–339. https://doi.org/10.1097/00010694-198612000-00001

Kozeny, J., 1927. Uber kapillare Leitung der Wasser in Boden. R. Acad. Sci., Vienna, Proc., 136, 271–306

Leij, F.J., Romano, N., Palladino, M., Schaap, M.G., Coppola, A., 2004. Topographical attributes to predict soil hydraulic properties along a hillslope transect. Water Resour. Res. 40(2), W02407. https://doi.org/10.1029/2002WR001641

Loague, K., 1992. Using soil texture to estimate saturated hydraulic conductivity and the impact on rainfall-runoff simulations. JAWRA J. Am. Water Resour. Assoc. 28(4), 687–693. https://doi.org/10.1111/j.1752-1688.1992.tb01490.x

McKeague, J.A., Wang C., Topp G.C., 1982. Estimating saturated hydraulic conductivity from soil morphology. Soil Sci. Soc. Am. J., 46(6), 1239–1244. https://doi.org/10.2136/sssaj1982.03615995004600060024x

Minasny, B., McBratney, A.B., Bristow, K.L., 1999. Comparison of different approaches to the development of pedotransfer functions for water-retention curves. Geoderma. 93(3), 225–253. https://doi.org/10.1016/S0016-7061(99)00061-0

Moret-Fernandez, D., Lopez, M., 2019. Determination of soil aggregate porosity using the modified water saturation method. Pedosphere. 29(6), 794–800. https://doi.org/10.1016/S1002-

0160(17)60427-2

Mualem, Y., 1976. A new model for predicting the hydraulic conductivity of unsaturated porous media. Water Resour. Res. 12(3), 513–522. https://doi.org/10.1029/WR012i003p00513

Nimmo, J.R., Herkelrath, W.N., Laguna Luna, A.M., 2007. Physically based estimation of soil water retention from textural data: General framework, new models, and streamlined existing models. Vadose Zone J. 6(4), 766–773. https://doi.org/10.2136/vzj2007.0019

Nimmo, J.R., Perkins, K.S., 2002. Aggregate stability and size distribution. in: Dane J.H., Topp C.G. (Eds.), Methods of Soil Analysis, Part 4: Physical Methods. Soil Science Society of America Inc., Madison, WI, pp. 317–328.

Othmer, H., Diekkrüger, B., Kutilek, M., 1991. Bimodal porosity and unsaturated hydraulic conductivity. Soil Sci. 152(3), 139–150. https://doi.org/10.1097/00010694-199109000-00001

Pachepsky, Y.A., Rawls, W.J., 2003. Soil structure and pedotransfer functions. Eur. J. Soil Sci. 54(3), 443–452. https://doi.org/10.1046/j.1365-2389.2003.00485.x

Pachepsky, Y.A., Smettem, K.R.J., Vanderborght, J., Herbst, M., Vereecken, H., Wosten, J.H.M., 2004. Reality and fiction of models and data in soil hydrology. in: Feddes, R. A., de Rooij, G.H., van Dam, J. C. (Eds.), Unsaturated-Zone Modeling: Progress, Challenges and Applications. Kluwer Academic Publishers, Dordrecht, pp. 231–260.

Priesack, E., Durner, W., 2006. Closed-form expression for the multi-modal unsaturated conductivity function. Vadose Zone J. 5(1), 121–124. https://doi.org/10.2136/vzj2005.0066

Rassam, D., Šimůnek, J., Van Genuchten, M.T., 2003. Modelling Variably Saturated Flow with HYDRUS-2D. ND Consult, Brisbane.

Rawls, W.J., Brakensiek, D.L., 1985. Prediction of soil water properties for hydrologic modeling, in:

Jones, E.B. (Ed), Watershed Management in the Eighties. American Society of Civil Engineers, New York.

Romano, N., Santini, A., 1997. Effectiveness of using pedo-transfer functions to quantify the spatial variability of soil water retention characteristics. J. Hydrol. 202(1), 137–157. https://doi.org/10.1016/S0022-1694(97)00056-5

Ross, P.J., Smettem, K.R.J., 1993. Describing soil hydraulic properties with sums of simple functions. Soil Sci. Soc. Am. J. 57(1), 26–29. https://doi.org/10.2136/sssaj1993.03615995005700010006x

Schaap, M.G., Bouten, W., 1996. Modeling water retention curves of sandy soils using neural networks. Water Resour. Res. 32(10), 3033–3040. https://doi.org/10.1029/96WR02278

Šimůnek, J., van Genuchten, M.T., 1996. Estimating unsaturated soil hydraulic properties from tension disc infiltrometer data by numerical inversion. Water Resour. Res. 32(9), 2683–2696. https://doi.org/10.1029/96WR01525

Šimůnek, J., van Genuchten, M.T., Šejna M., 2008. Development and applications of the HYDRUS and STANMOD software packages and related codes. Vadose Zone J. 7(2), 587–600. https://doi.org/10.2136/vzj2007.0077

Sobieraj, J.A., Elsenbeer, H., Vertessy R.A., 2001. Pedotransfer functions for estimating saturated hydraulic conductivity: implications for modeling storm flow generation. J. Hydrol. 251(3), 202–220. https://doi.org/10.1016/S0022-1694(01)00469-3

Sposito, G., 1998. Scale Dependence and Scale Invariance in Hydrology. Cambridge University Press, Cambridge.

Tietje, O., Hennings V., 1996. Accuracy of the saturated hydraulic conductivity prediction by pedo-transfer functions compared to the variability within FAO textural classes. Geoderma, 69(1), 71–84. https://doi.org/10.1016/0016-7061(95)00050-X

Timlin, D.J., Ahuja, L.R., Pachepsky, Y., Williams, R.D., Gimenez, D., Rawls, W., 1999. Use of Brooks-Corey parameters to improve estimates of saturated conductivity from effective porosity. Soil Sci. Soc. Am. J. 63(5), 1086–1092. https://doi.org/10.2136/sssaj1999.6351086x

Van Dam, J.C., Huygen, J., Wesseling, J.G., Feddes, R.A., Kabat, P., Van Walsum, P.E., Groenendijk, P., Van Diepen, C.A., 1997. Theory Of SWAP Version 2.0; Simulation of Water Flow, Solute Transport and Plant Growth in the Soil-Water-Atmosphere-Plant Environment. Waginengen Agricultural University and DLO Winand Staring Centre, Waginengen.

van Genuchten, M.T., 1980. A closed-form equation for predicting the hydraulic conductivity of unsaturated soils. Soil Sci. Soc. Am. J. 44(5), 892–898. https://doi.org/10.2136/sssaj1980.03615995004400050002x

van Genuchten, M.T., Nielsen, R., 1985. On describing and predicting the hydraulic properties. Ann. Geophys. 3(5), 615–628.

Vereecken, H., Weynants, M., Javaux, M., Pachepsky, Y., Schaap, M.G., van Genuchten, M.T., 2010. Using pedotransfer functions to estimate the van Genuchten–Mualem soil hydraulic properties: A review. Vadose Zone J. 9(4), 795–820. https://doi.org/10.2136/vzj2010.0045

Vogel, T., Cislerova, M., 1988. On the reliability of unsaturated hydraulic conductivity calculated from the moisture retention curve. Transp. Porous Media. 3(1), 1–15. https://doi.org/10.1007/BF00222683

Wilson, G. V., Jardine, P.M., Gwo, J.P., 1992. Modeling the hydraulic properties of a multiregion soil. Soil Sci. Soc. Am. J. 56(6), 1731–1737. https://doi.org/10.2136/sssaj1992.03615995005600060012x

Tables

Table 1. Mean (μ) and standard deviations (σ) of measured (subscrip *meas*) and AP PTF (subscript *PTF*) hydraulic parameters obtained from unimodal and bimodal inverse models. The scaling parameter, α_{AP}, is also reported only for the PTF case

Parameter	μ_{meas}	σ_{meas}	μ_{PTF}	σ_{PTF}	Scenario
α	0.137	0.129	0.192	0.439	**Unimodal**
n	1.476	0.431	1.273	0.187	
K_0 (cm/min)	2.367	15.062	0.171	0.193	
α_{AP}	-	-	1.269	0.264	
α_1	0.590	1.055	2.249	2.204	**Bimodal**
n_1	2.569	2.160	3.127	2.522	
α_2	0.049	0.042	0.042	0.126	
n_2	1.496	0.423	1.539	0.126	
K_0 (cm/min)	0.266	0.915	0.206	0.434	
α_{AP}	-	-	1.156	0.311	

Table 2: Results of MLR application to predict the α_{AP} parameter from soil physical parameters. Subscript PSD and ASD stand for particle and aggregate size distribution, respectively

MLR Parameter	Coefficients	Lower 95%	Upper 95%	Scenario
Intercept	9.939	3.031	16.847	
ρ_b (g/cm^3)	0.480	-0.104	1.063	
$T_{s,PSD}$	0.007	-0.043	0.057	**Unimodal**
$T_{\alpha,PSD}$	0.002	-0.003	0.007	
$T_{n,PSD}$	-11.835	-20.893	-2.777	
Intercept	-5.398	-15.139	3.105	
ρ_b (g/cm^3)	0.684	-0.056	1.424	
$T_{s,PSD}$	-0.028	-0.107	0.051	
$T_{\alpha,PSD}$	0.000	-0.006	0.007	
$T_{n,PSD}$	9.902	-0.751	20.554	**Bimodal**
$T_{s,ASD}$	-0.009	-0.034	0.016	
$T_{\alpha,ASD}$	0.934	-1.430	3.298	
$T_{n,ASD}$	0.006	-0.025	0.037	
β_1	-0.619	-1.552	2.790	

Abstract: The main purpose of this paper is to develop a bimodal pedotransfer function to obtain soil water retention (WRC) and hydraulic conductivity (HCC) curves. The proposed pedo-transfer function (PTF) extends the Arya and Paris (AP) approach, which is based on particle size distribution (PSD), by incorporating aggregate-size distribution (ASD) into the PTF to obtain the bimodal WRC. A bimodal porosity approach was developed to quantify the fraction of each of the porous systems (matrix and macropores) in overall soil porosity. Saturated hydraulic conductivity, K_0, was obtained from WRC using the Kozeny-Carman equation, whose parameters were inferred from the behaviour of the bimodal WRC close to saturation. Finally, the Mualem model was applied to obtain the HCC. In order to calibrate the PTF, measured soil physical and hydraulic properties data were used, coming from field infiltration experiments from an irrigation sector of 140 ha area in the "Sinistra Ofanto" irrigation system in Apulia, southern Italy. The infiltration data were fitted by using both bimodal and unimodal hydraulic properties by an inverse solution of the Richards equation. The bimodal "measured" hydraulic properties were then used to calibrate the scaling parameter (α_{AP}) of the proposed bimodal AP (*bimAP*) PTF. Similarly, for the sake of comparison with the bimodal results, the unimodal hydraulic properties were used to calibrate the α_{AP} of the classical unimodal AP (*unimAP*) PTF. Compared to the *unimAP* PTF, the proposed *bimAP* significantly improves the predictions of the mean WRC parameters and K_0, as well as the prediction of the shape of the whole HCC. Moreover, compared to the unimodal approach, it also allows keeping the hydraulic parameters' spatial variability observed in the calibration dataset. Multiple linear regression (MLR) was also applied to analyse the sensitivity of the bimodal α_{AP} parameter to textural and structural features, confirming significant predictive effects of soil structure.

Highlights

- Bimodal Arya&Paris hydraulic properties were developed based on soil structure
- The bimodal PTF provides better prediction of un/saturated hydraulic conductivity
- The bimodal PTF keeps the spatial variability of the original hydraulic properties

Declaration of interests

☒The authors declare that they have no known competing financial interests or personal relationships that could have appeared to influence the work reported in this paper.

☐The authors declare the following financial interests/personal relationships which may be considered as potential competing interests:

Figure 1

Click here to access/download;Figure;Figure 1.tif

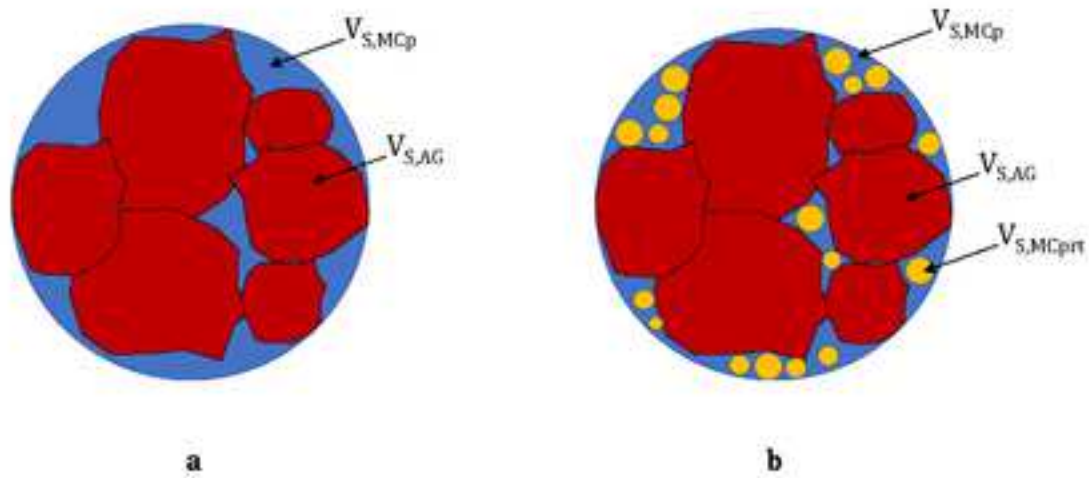

Figure 2

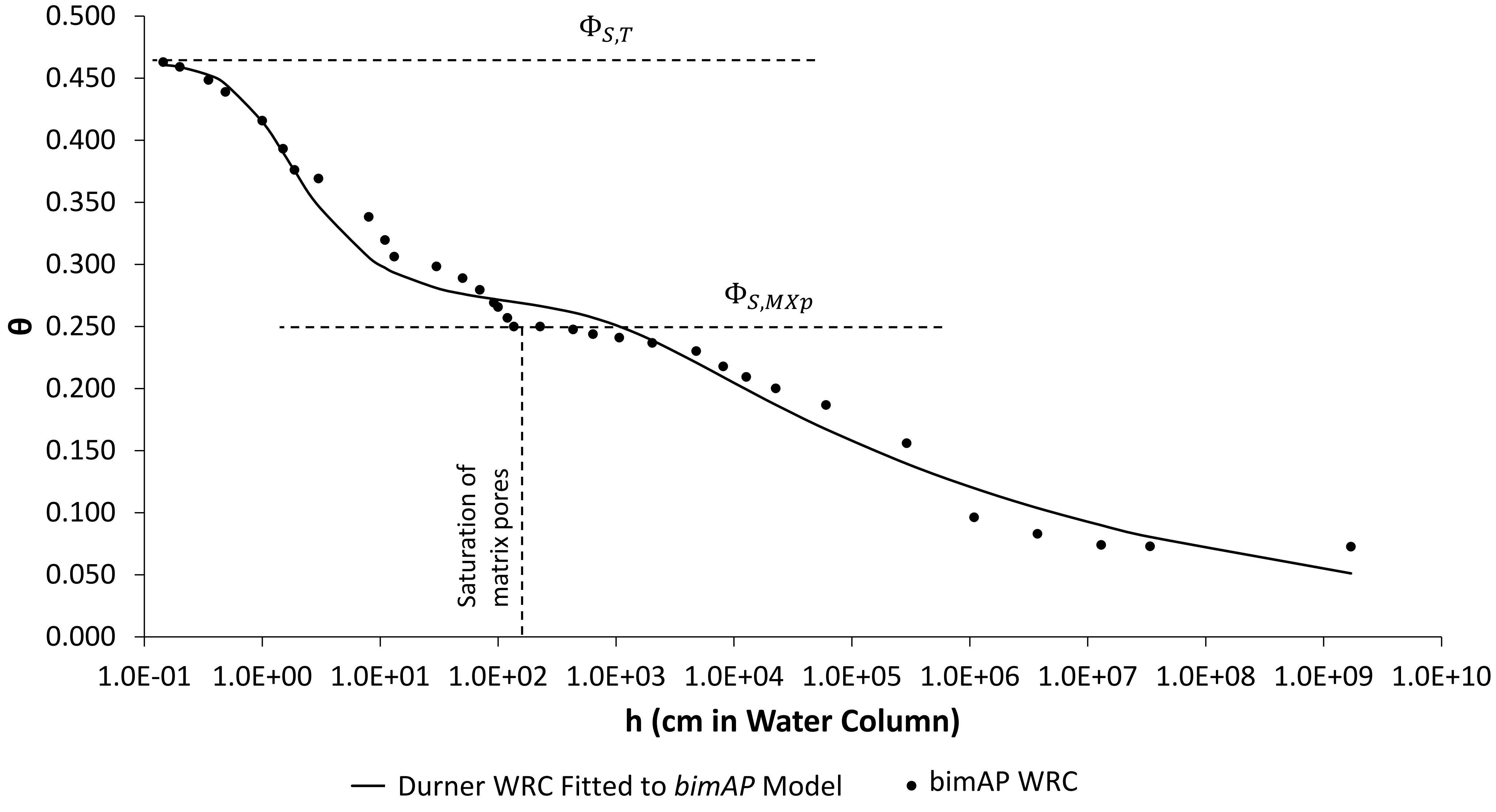

$\Phi_{S,T}$
$\Phi_{S,MXp}$
θ
0.500
0.450
0.400
0.350
0.300
0.250
0.200
0.150
0.100
0.050
0.000
Saturation of matrix pores
1.0E-01
1.0E+00
1.0E+01
1.0E+02
1.0E+03
1.0E+04
1.0E+05
1.0E+06
1.0E+07
1.0E+08
1.0E+09
1.0E+10
h (cm in Water Column)
Durner WRC Fitted to *bimAP* Model
bimAP WRC

Figure 3 Click here to access/download;Figure;Figure 3.jpg

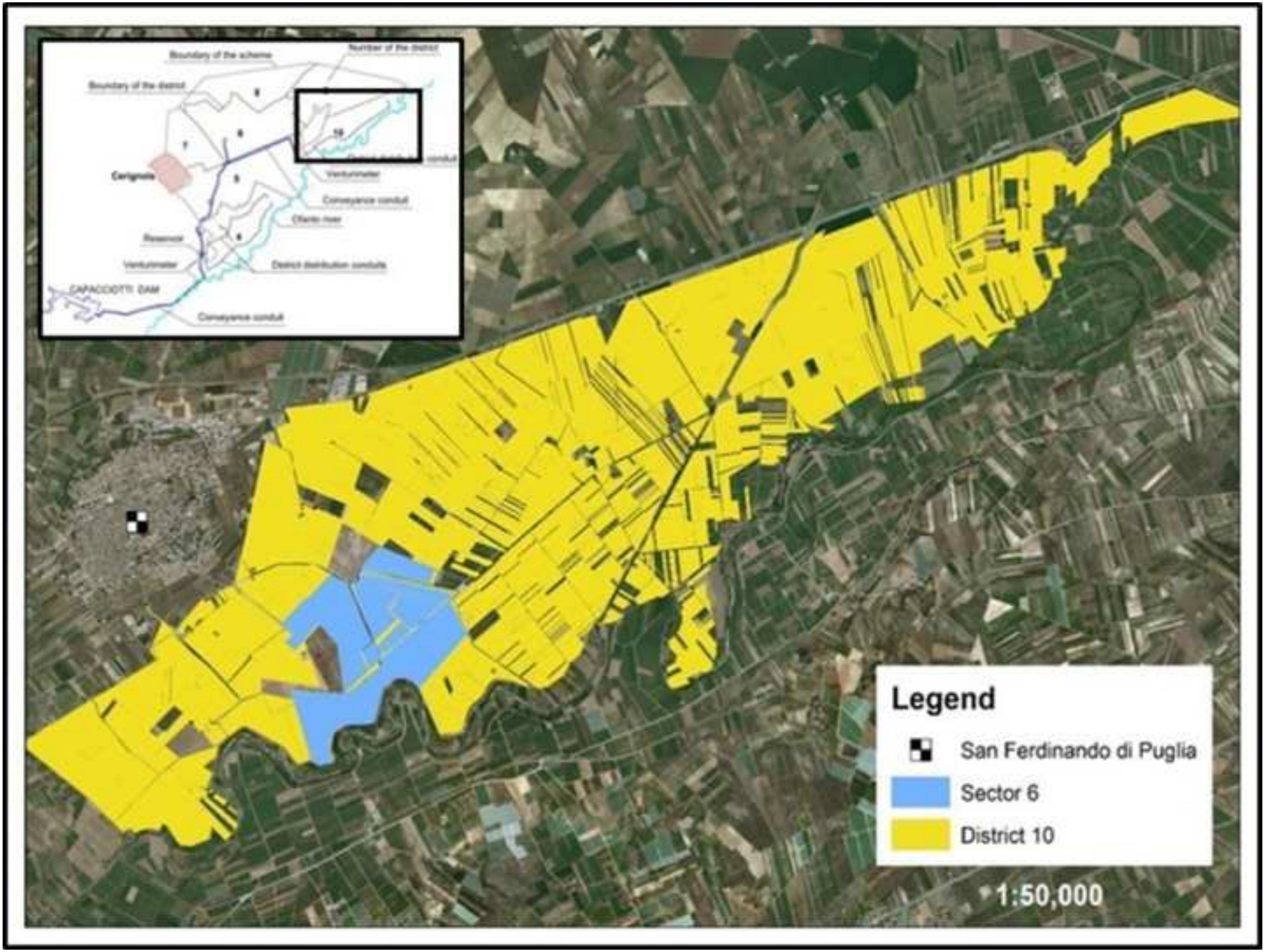

Figure 4

Click here to access/download;Figure;Figure 4.tif

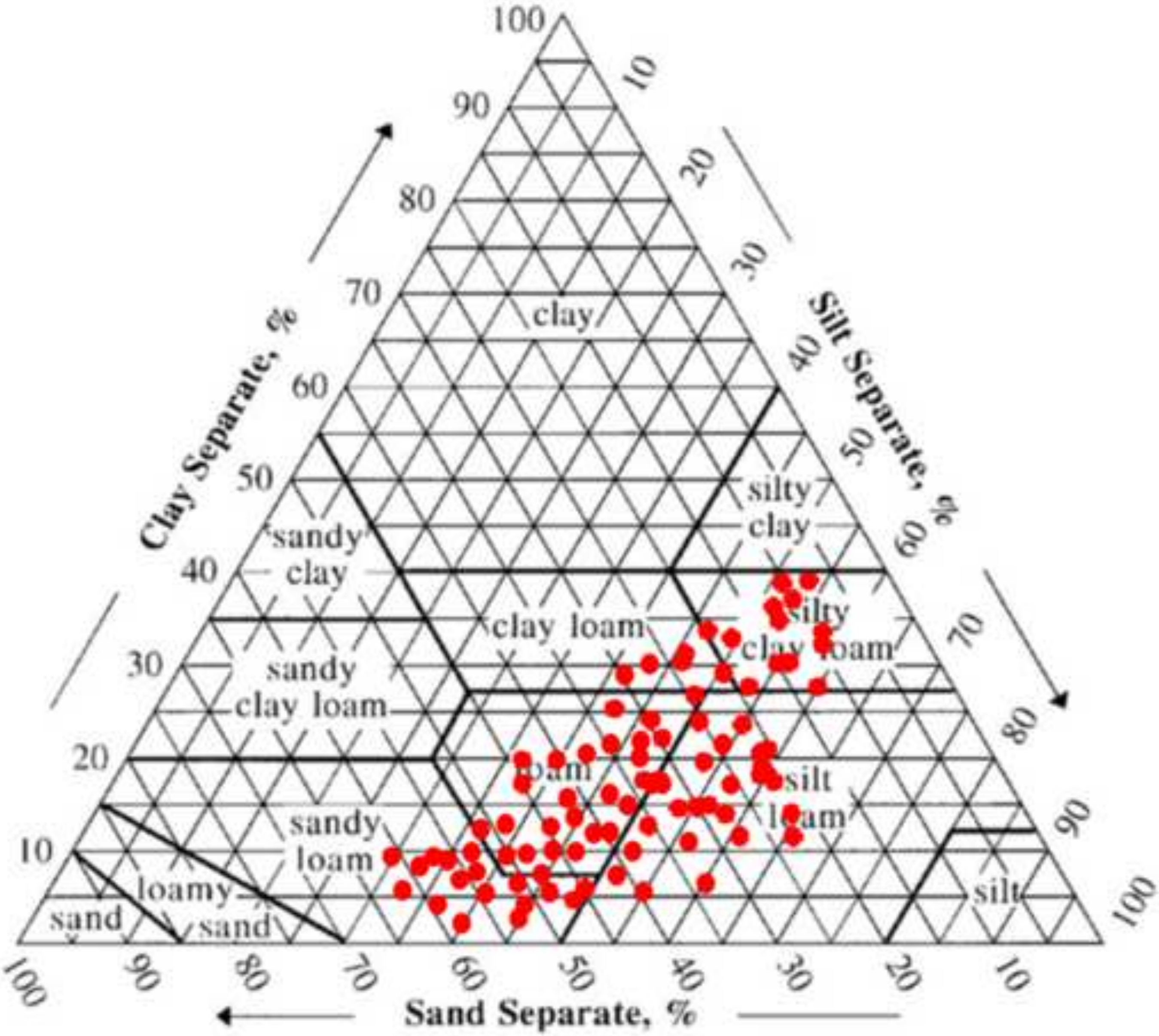

Figure 5

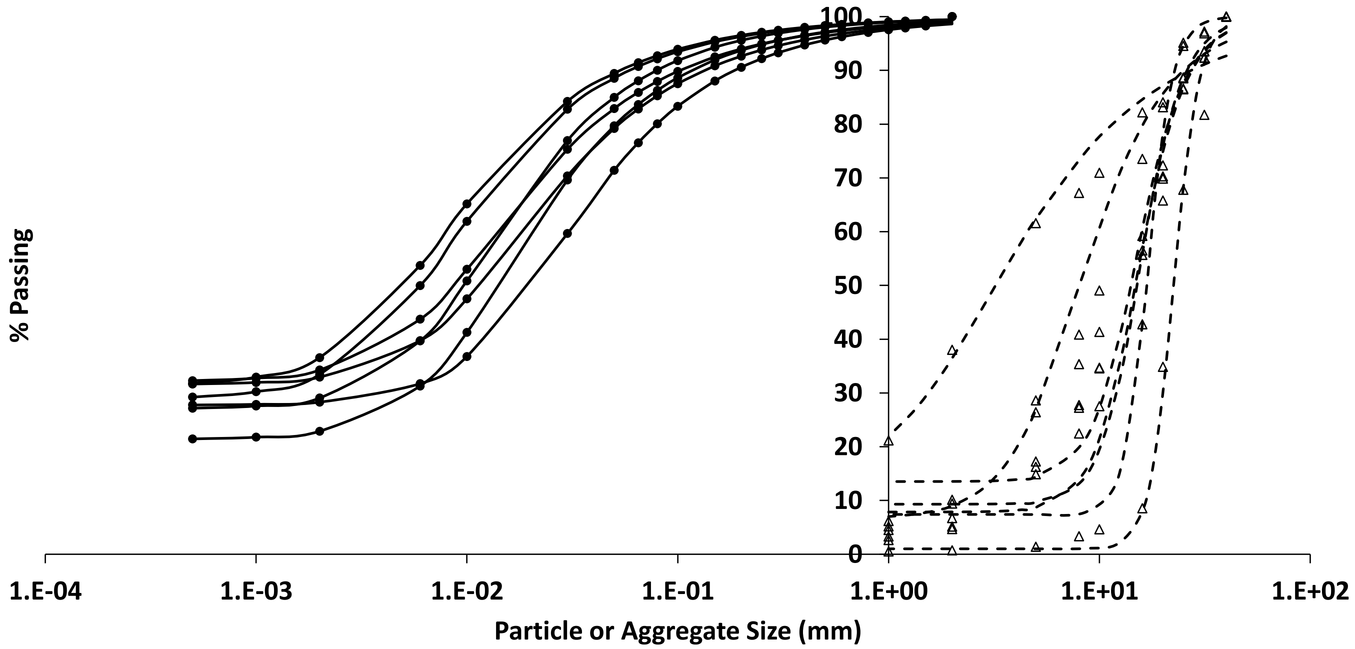

% Passing
100
90
80
70
60
50
40
30
20
10
0
1.E-04
1.E-03
1.E-02
1.E-01
1.E+00
1.E+01
1.E+02
Particle or Aggregate Size (mm)

Figure 6

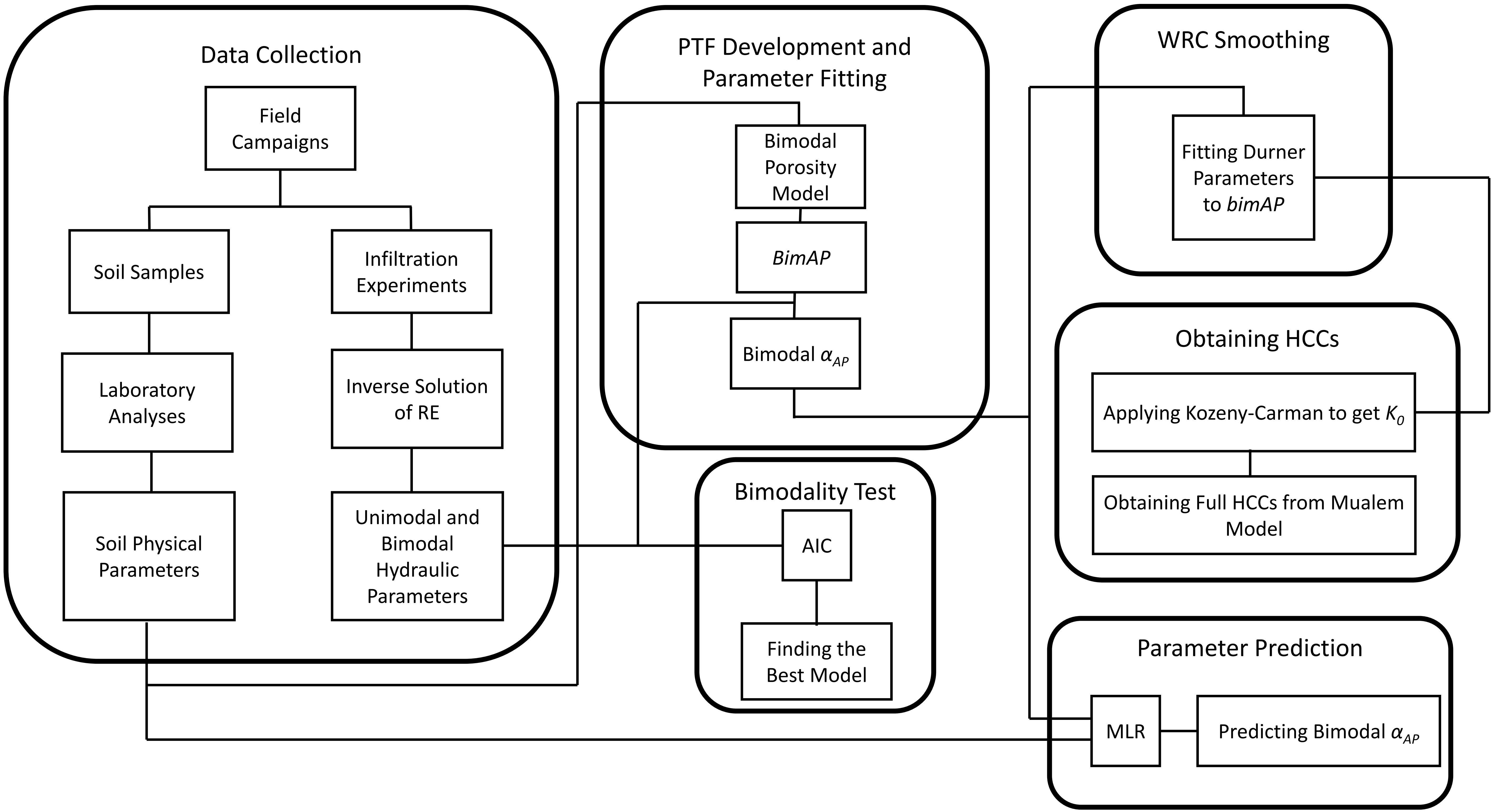

Data Collection
Field Campaigns
Soil Samples
Infiltration Experiments
Laboratory Analyses
Inverse Solution of RE
Soil Physical Parameters
Unimodal and Bimodal Hydraulic Parameters
PTF Development and Parameter Fitting
Bimodal Porosity Model
BimAP
Bimodal α_{AP}
Bimodality Test
AIC
Finding the Best Model
WRC Smoothing
Fitting Durner Parameters to *bimAP*
Obtaining HCCs
Applying Kozeny-Carman to get K_0
Obtaining Full HCCs from Mualem Model
Parameter Prediction
MLR
Predicting Bimodal α_{AP}

Figure 7

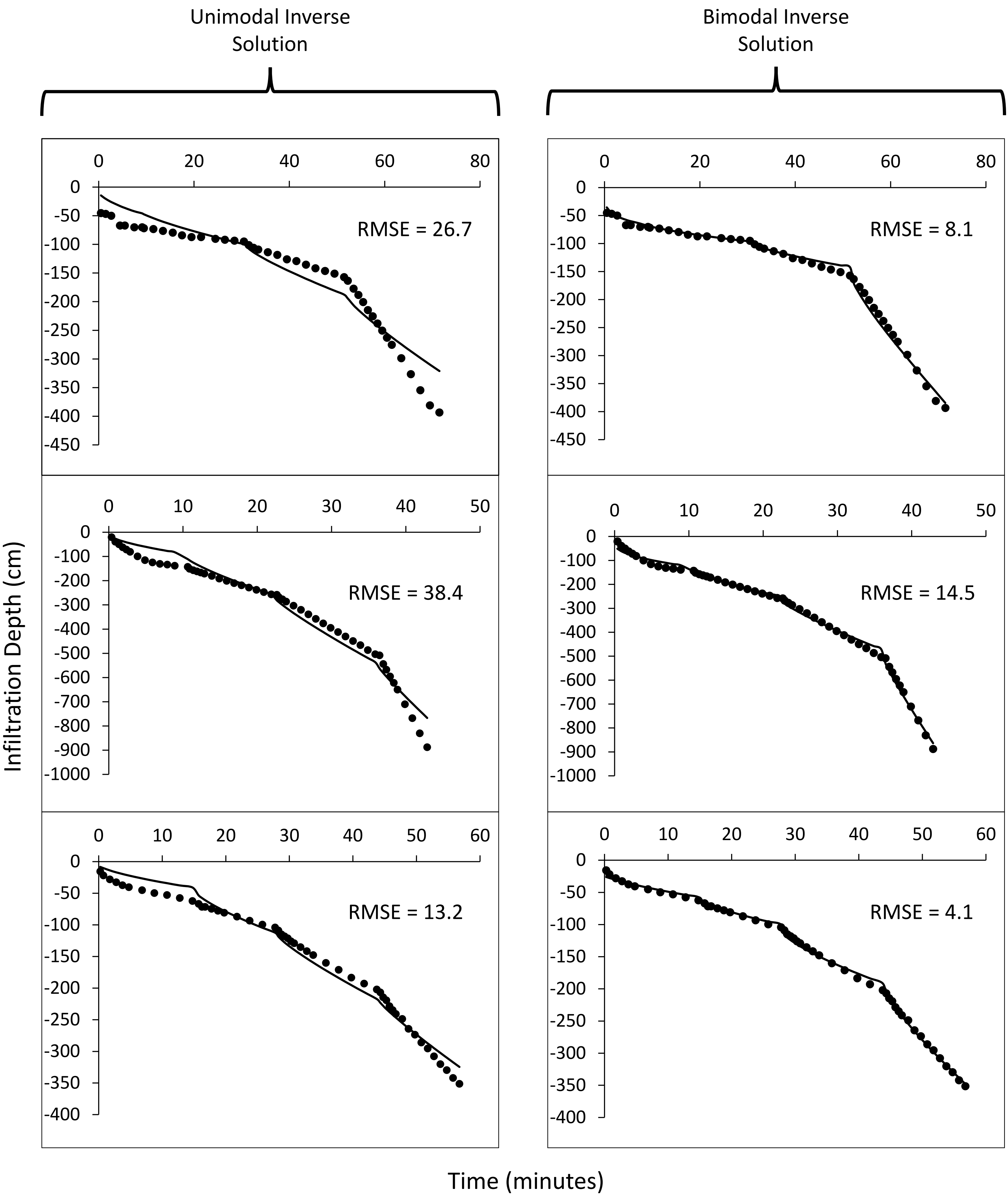
Unimodal Inverse Solution
Bimodal Inverse Solution
RMSE = 26.7
RMSE = 8.1
RMSE = 38.4
RMSE = 14.5
RMSE = 13.2
RMSE = 4.1
Infiltration Depth (cm)
Time (minutes)

Figure 8

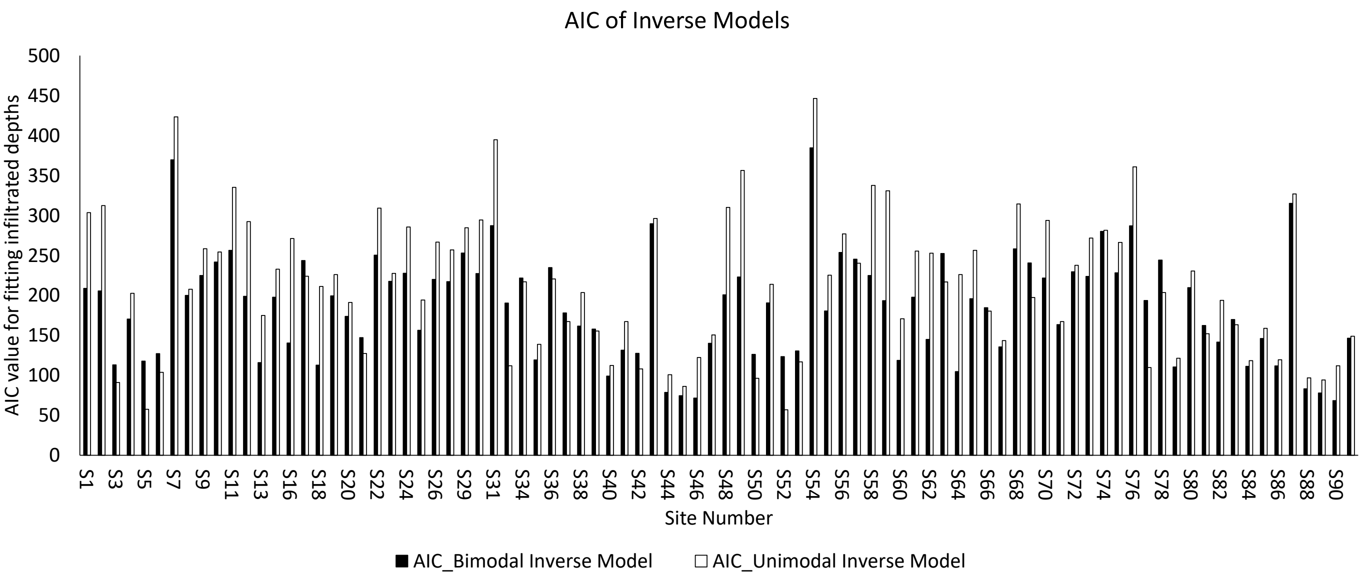

AIC of Inverse Models
AIC value for fitting infiltrated depths
500
450
400
350
300
250
200
150
100
50
0
S1
S3
S5
S7
S9
S11
S13
S16
S18
S20
S22
S24
S26
S29
S31
S34
S36
S38
S40
S42
S44
S46
S48
S50
S52
S54
S56
S58
S60
S62
S64
S66
S68
S70
S72
S74
S76
S78
S80
S82
S84
S86
S88
S90
Site Number
AIC_Bimodal Inverse Model
AIC_Unimodal Inverse Model

Figure 9

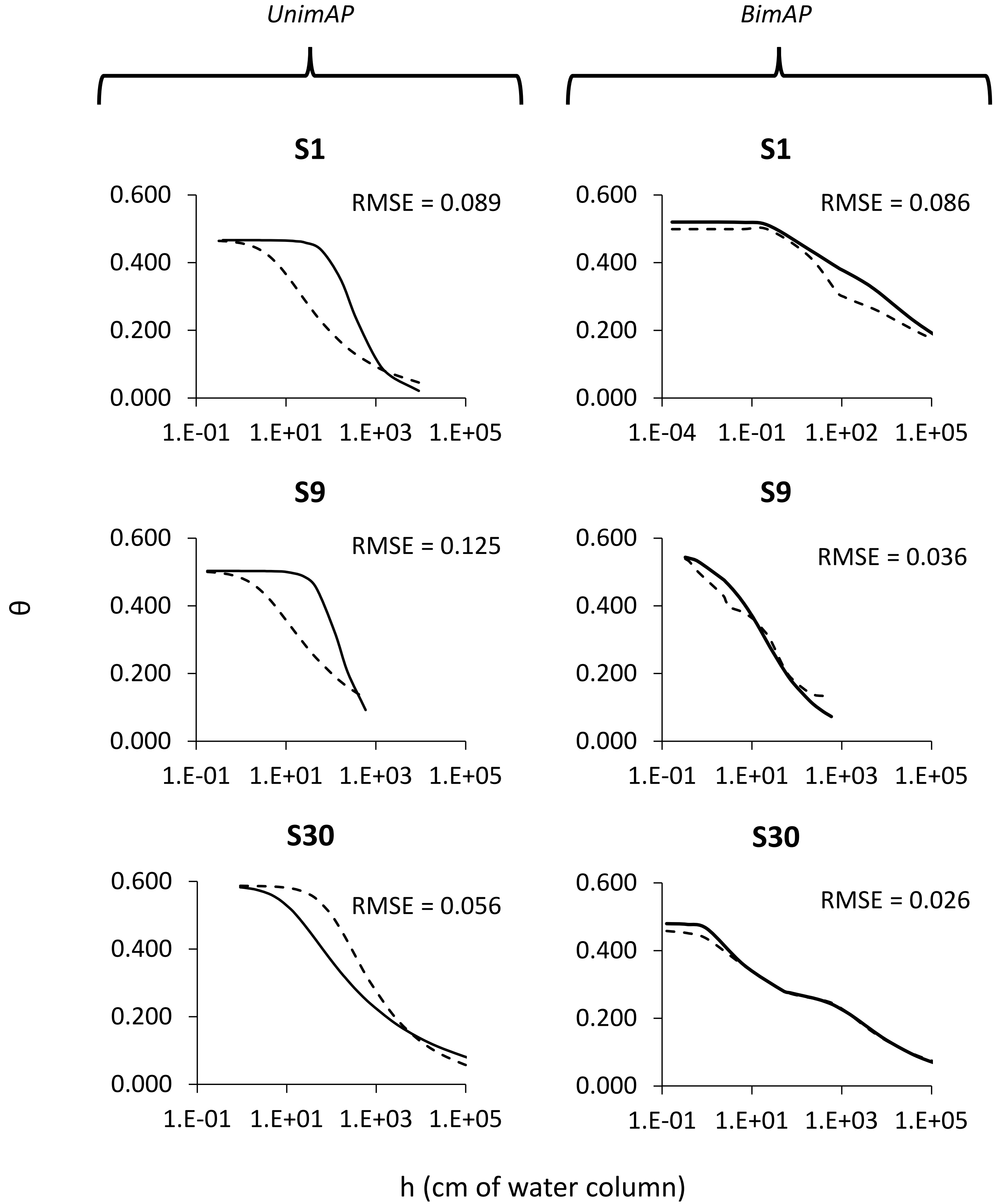
UnimAP
BimAP
S1
RMSE = 0.089
S1
RMSE = 0.086
S9
RMSE = 0.125
S9
RMSE = 0.036
S30
RMSE = 0.056
S30
RMSE = 0.026
θ
h (cm of water column)
0.600
0.400
0.200
0.000
1.E-01
1.E+01
1.E+03
1.E+05
1.E-04
1.E+02

Figure 10

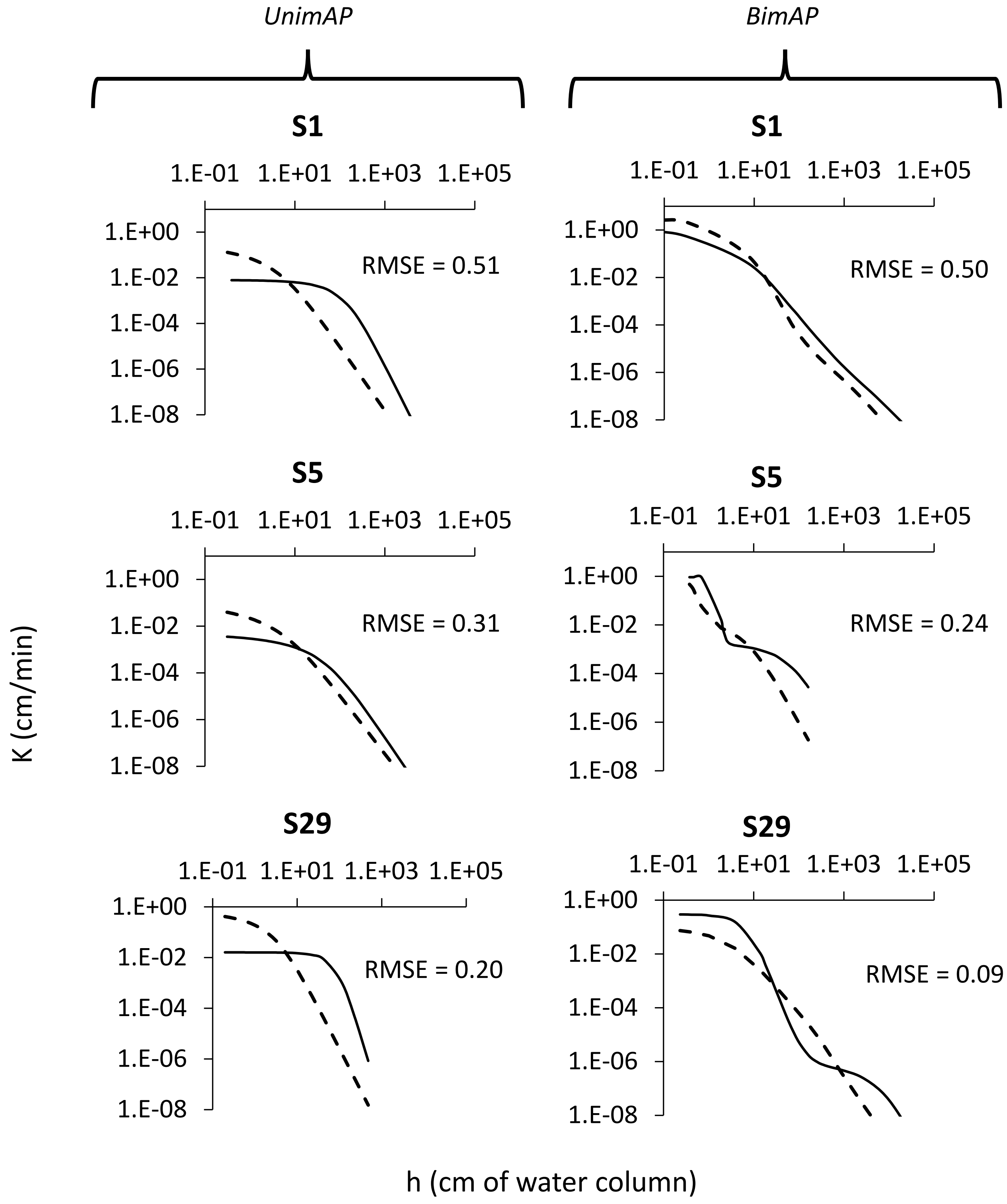

UnimAP
BimAP
S1
S1
1.E-01
1.E+01
1.E+03
1.E+05
1.E+00
1.E-02
1.E-04
1.E-06
1.E-08
RMSE = 0.51
RMSE = 0.50
S5
S5
RMSE = 0.31
RMSE = 0.24
S29
S29
RMSE = 0.20
RMSE = 0.09
K (cm/min)
h (cm of water column)

Figure 11

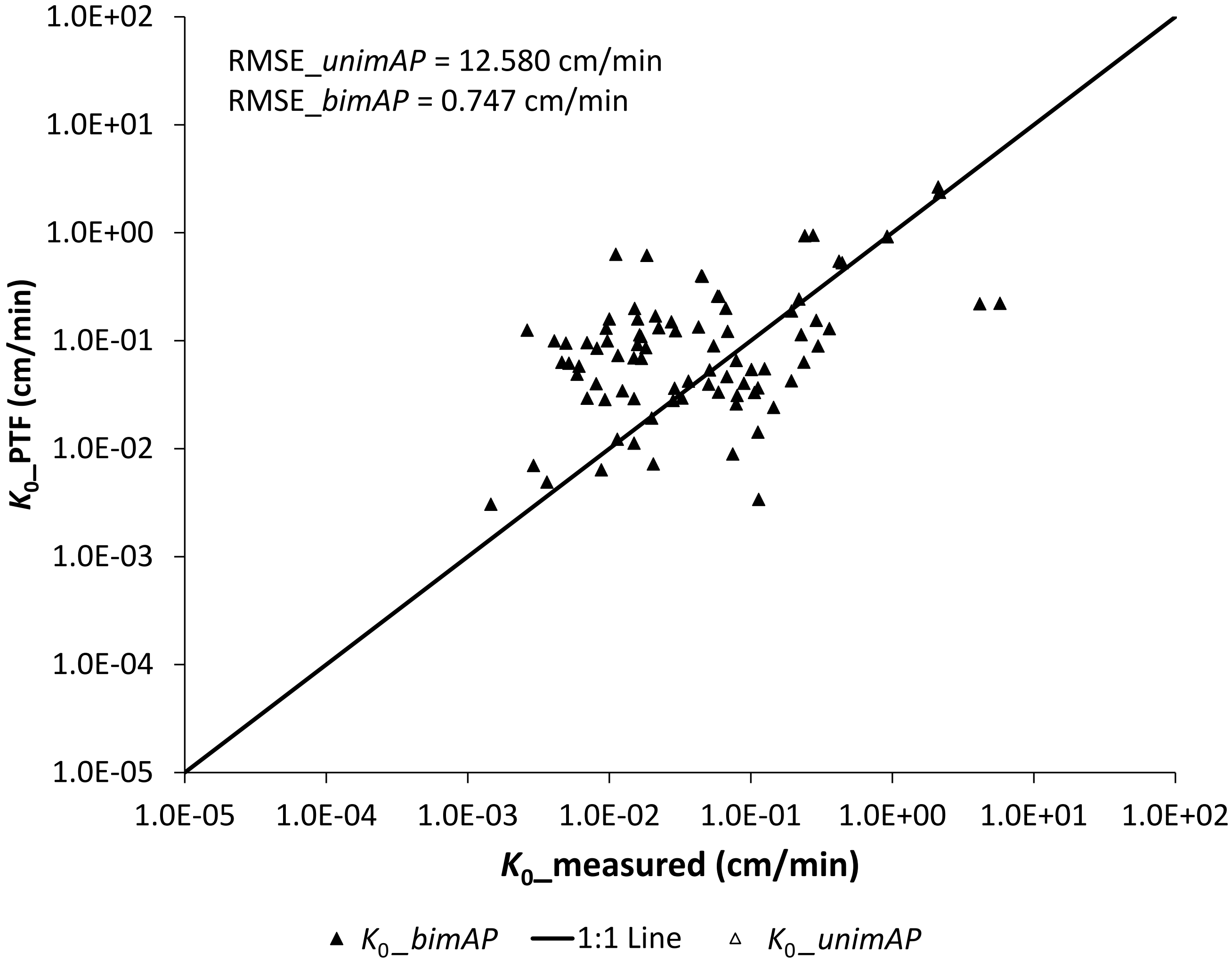

RMSE_*unimAP* = 12.580 cm/min
RMSE_*bimAP* = 0.747 cm/min
1.0E+02
1.0E+01
1.0E+00
1.0E-01
1.0E-02
1.0E-03
1.0E-04
1.0E-05
K_0_PTF (cm/min)
1.0E-05
1.0E-04
1.0E-03
1.0E-02
1.0E-01
1.0E+00
1.0E+01
1.0E+02
K_0_measured (cm/min)
K_0_*bimAP*
1:1 Line
K_0_*unimAP*

Figure 12

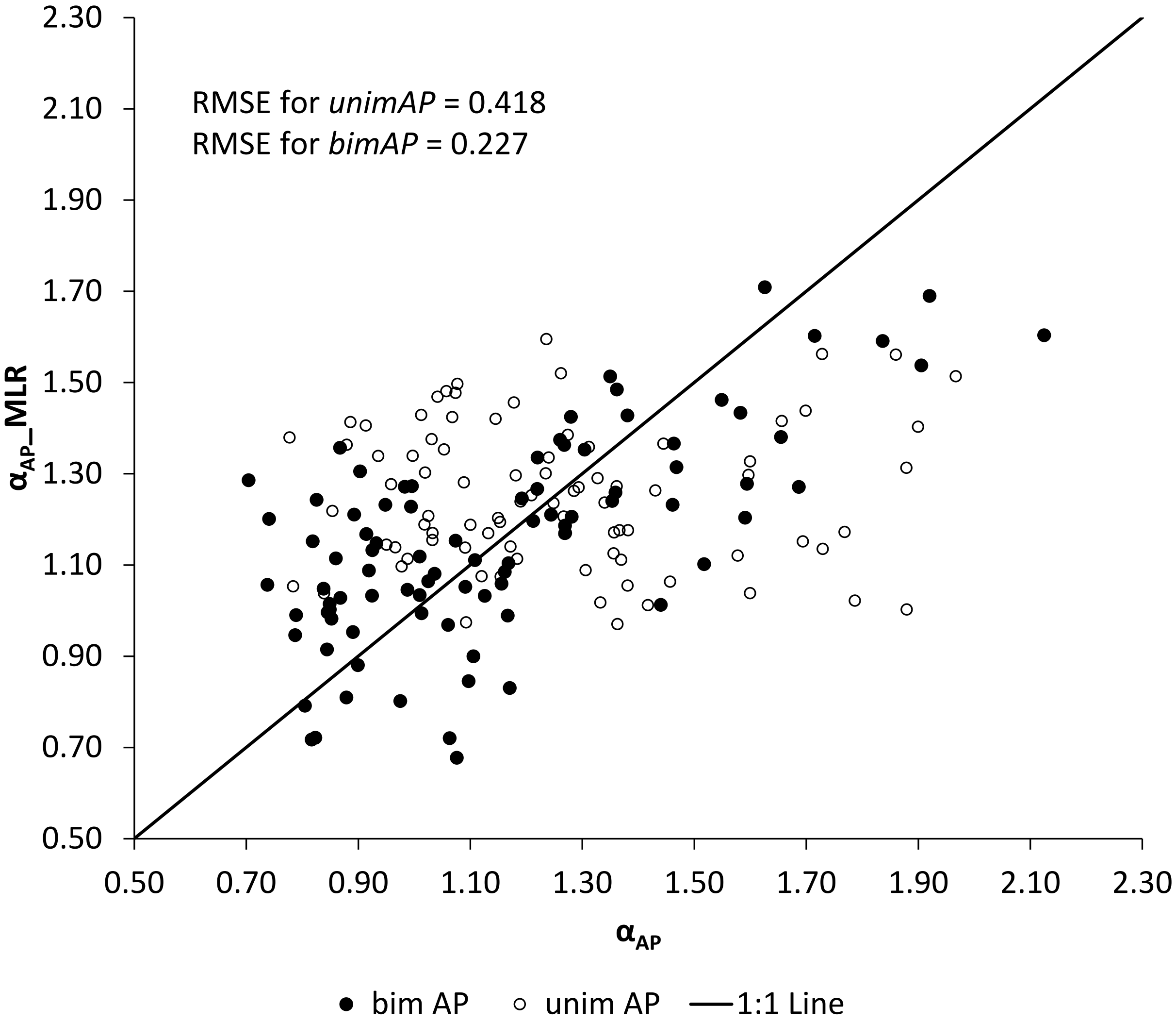

RMSE for *unimAP* = 0.418
RMSE for *bimAP* = 0.227
2.30
2.10
1.90
1.70
1.50
1.30
1.10
0.90
0.70
0.50
0.50
0.70
0.90
1.10
1.30
1.50
1.70
1.90
2.10
2.30
αAP_MLR
αAP
bim AP
unim AP
1:1 Line

Figure 1. Schematic view of an undisturbed sample consisting: a) only of aggregates, without particle inclusions in the interspace among the aggregates; b) of aggregates with particle inclusions (orange circles) in the interspace among the aggregates

Figure 2. The bimAP WRC (symbols) and the measured bimodal WRC (solid line). The structural and textural parts of the WRC are clearly visible in both the curves. The two horizontal dashed lines indicate the porosity of the structural and textural regions of the bimAP WRC

Figure 3. The study area, the sector 6 of the district 10 in "Sinistra Ofanto" irrigation system

Figure 4. USDA textures of the 90 soil samples considered in this paper

Figure 5. Measured and fitted PSDs and ASDs for 7 of the samples used in the study. The divide between PSDs and ASDs is at 1 mm size. The symbols represent the measured data while the curves represent the curves fitted to equation (30).

Figure 6. Schematic view of steps followed to develop *bimAP* WRCs, HCCs, and predict *bimAP* scaling parameters (α_{AP})

Figure 7. Inverse solution results for three 3 locations in the study area. The symbols and solid lines represent the observed infiltration depths and the infiltration depths obtained from the inverse solution using DISC for the unimodal case (plots on the left) and HYDRUS 3D for the bimodal case (plots on the rigth)

Figure 8. Akaike's Information Criterion (AIC) value resulting from fitting measured infiltrated depths to Richard's infiltration model using the unimodal van Genuchten model (blank bars) and the bimodal Durner model (black bars) in all the ninety sites.

Figure 9. Comparison of the measured WRCs (solid lines - coming from the inversion of infiltration

experiments) to those obtained by both the *unimAP* and the *bimAP* (dashed lines) for three of the sites investigated. The graphs on the left side compare unimodal measured and estimated WRCs, those on the right side compare bimodal measured and estimated WRCs.

Figure 10. Comparison of the measured HCCs (solid lines - coming from the inversion of infiltration experiments) to those obtained by both the *unimAP* and the *bimAP* (dashed lines) for three of the sites investigated. The graphs on the left side compare unimodal measured and estimated HCCs, those on the right side compare bimodal measured and estimated HCCs.

Figure 11. K_0 obtained from *bimAP* and *unimAP* plotted against K_0 obtained from bimodal and unimodal inverse solutions respectively. The empty triangles represent the unimodal scenario and solid triangles represent the bimodal scenario. The solid line is a 1:1 line.

Figure 12. The α_{AP} values obtained by the MLR against the original values of α_{AP} for both the *unimAP* (white symbols) and *bimAP* (black symbols) approaches.

Table 1. Mean (μ) and standard deviations (σ) of measured (subscrip *meas*) and AP PTF (subscript *PTF*) hydraulic parameters obtained from unimodal and bimodal inverse models. The scaling parameter, α_{AP}, is also reported only for the PTF case

Parameter	μ_{meas}	σ_{meas}	μ_{PTF}	σ_{PTF}	**Scenario**
α	0.137	0.129	0.192	0.439	Unimodal
n	1.476	0.431	1.273	0.187	
K_0 (cm/min)	2.367	15.062	0.171	0.193	
α_{AP}	-	-	1.269	0.264	
α_1	0.590	1.055	2.249	2.204	Bimodal
n_1	2.569	2.160	3.127	2.522	
α_2	0.049	0.042	0.042	0.126	
n_2	1.496	0.423	1.539	0.126	
K_0 (cm/min)	0.266	0.915	0.206	0.434	
α_{AP}	-	-	1.156	0.311	

Table 1: Results of MLR application to predict the α_{AP} parameter from soil physical parameters. Subscript PSD and ASD stand for particle and aggregate size distribution, respectively

MLR Parameter	Coefficients	Lower 95%	Upper 95%	Scenario
Intercept	9.939	3.031	16.847	**Unimodal**
ρ_b (g/cm^3)	0.480	-0.104	1.063	
$T_{s,PSD}$	0.007	-0.043	0.057	
$T_{\alpha,PSD}$	0.002	-0.003	0.007	
$T_{n,PSD}$	-11.835	-20.893	-2.777	
Intercept	-5.398	-15.139	3.105	**Bimodal**
ρ_b (g/cm^3)	0.684	-0.056	1.424	
$T_{s,PSD}$	-0.028	-0.107	0.051	
$T_{\alpha,PSD}$	0.000	-0.006	0.007	
$T_{n,PSD}$	9.902	-0.751	20.554	
$T_{s,ASD}$	-0.009	-0.034	0.016	
$T_{\alpha,ASD}$	0.934	-1.430	3.298	
$T_{n,ASD}$	0.006	-0.025	0.037	
β_1	-0.619	-1.552	2.790	